Available online at www.sciencedirect.com
ScienceDirect
PROGRESS IN HISTOCHEMISTRY AND CYTOCHEMISTRY
ELSEVIER Progress in Histochemistry and Cytochemistry 44 (2009) 125–172
www.elsevier.de/proghi

Recent advances in quantitative colocalization analysis: Focus on neuroscience

Vadim Zinchuk[a,*], Olga Grossenbacher-Zinchuk[b]

[a]*Department of Anatomy and Cell Biology, Kochi University Faculty of Medicine, Kohasu, Okoh-cho, Nankoku, Kochi 783-8505, Japan*
[b]*Department of Medicine, Unit of Anatomy, Fribourg University, Fribourg, Switzerland*

Abstract

Quantitative colocalization analysis is an advanced digital imaging tool to characterize the spatial expression of molecules of interest in immunofluorescence images obtained using confocal microscopes. It began from simple pixel counting and, with introduction of specialized algorithms, transformed into a powerful image analyzing technique capable of

Abbreviations: AMPA, alpha-amino-3-hydroxy-5-methyl-4-isoxazolepropionic acid; AMPAR, AMPA receptor; AP, alkaline phosphatase; BF, buoyant fraction; CeA, central nucleus of amygdala; CT-B, cholera toxin B; DAPI, 4′,6-diamidino-2-phenylindole; DA, dopamine; EGFP, enhanced green fluorescent protein; EYFP, enhanced yellow fluorescent protein; ERK, extracellular signal-regulated kinase; FISH, fluorescence in situ hybridization; FITC, fluorescein iso-thiocyanate; FRET, fluorescence resonance energy transfer; GABA, gamma-aminobutyric acid; GAD67, glutamic acid decarboxylase of 67 kDa; GFP, green fluorescent protein; HF, heavy fraction; HTML, hypertext markup language; LTD, long-term depression; LTP, long-term potentiation; MD, monocular visual deprivation; MOC, Manders' overlap coefficient; mRNA, messenger ribonucleic acid; NK1, neurokinin1; NMDA, N-methyl-D-aspartic acid; NMDAR, N-methyl-D-aspartate receptor; NMDAR2B, NMDAR type 2B; NSF, N-ethylmaleimide sensitive fusion protein; PCC, Pearson's correlation coefficient; PDF, portable document format; PFC, prefrontal cortex; RNP, ribonucleoprotein; ROI, region of interest; SFK, Src tyrosine kinase; SMA, spinal muscular atrophy; SMN, survival of motor neuron protein; SNAP-25, synaptosomal-associated protein of 25 KDa; SNARE, SNAP and NSF attachment receptors; snRNP, small nuclear ribonucleoprotein; SP, substance P; TBS, tris-buffered saline; TIFF, tagged image file format; TLS, translocated in liposarcoma; TLS-KO, TLS knock out; TRITC, tetramethyl rhodamine iso-thiocyanate; VAMP, vesicle-associated membrane protein; VGAT, vesicular GABA transporter; VGLUT, vesicular glutamate transporter; VTA, ventral tegmental area; YFP, yellow fluorescent protein.

*Corresponding author. Tel.: +81 88 880 2302; fax: +81 88 880 2304.
E-mail address: zinchuk@s.kochi-u.ac.jp (V. Zinchuk).

0079-6336/$ - see front matter © 2009 Published by Elsevier GmbH.
doi:10.1016/j.proghi.2009.03.001

identifying the exact locations of various molecules in tissues and cells and describing their subtle changes in dynamics. Applications of quantitative colocalization in the field of neuroscience proved to be particularly informative by helping to obtain observations not otherwise achievable using other techniques. In this article, we review the background and applicability of quantitative colocalization with special focus on neuroscience research.

1. Introduction

In the recent years, we are witnessing an explosive increase in the use of quantitative imaging techniques in cell and molecular biological studies. Quantitative approach became so widely popular, because it not only allows to extend the significance of qualitative observations, but also helps to obtain unique and crucially important results (Halbhuber and Konig, 2003; Oberholzer et al., 1996). Although performing quantitative analysis of images frequently requires more effort in experimental design and methodology than comparable qualitative assessments, it is usually fully justified by the importance of quantitative findings (Fricker et al., 2006). This is especially true when the applied quantitative methodology allows comparison of the data obtained in different laboratories as well as ensures smooth integration of imaging and statistical information.

Colocalization analysis is one of the biggest winners in the use of quantitative approach, because quantification of colocalization has the potential to bridge the gap between its subjective observations and actual measurements. Colocalization is important as it is one of the most frequently reported visual phenomena in modern cell and molecular biological research. Finding of colocalization is used to identify the exact location of the structures of interest and lends support for envisioning their common characteristics. Colocalization of molecules is governed by fundamental biological mechanisms, such as compartmentalization and binding. These processes target various molecules to specific locations in cells and let them colocalize (Kuriyan and Eisenberg, 2007). Colocalization is also critical for understanding the essence of transcriptional control, metabolism, and various signaling events (Pawson and Scott, 1997). It occurs when two or more antigens are visualized in the same section using corresponding fluorescence-labeled secondary antibodies with different excitation spectra. Overlap of these spectra will eventually result in the appearance of colocalization (Smallcombe, 2001).

In this review, we focus on advances in quantitative colocalization analysis and its applications in the field of neuroscience. Among a considerable number of neuroscience articles reporting quantification of colocalization observations, we paid particular attention to those providing the most insightful and, equally important, readily reproducible examples of the practical use of the technique. We also aimed to showcase examples that address important biological questions by efficiently combining quantification of colocalization with other analytical techniques.

1.1. Definition of colocalization

Definition of colocalization depends on how it is examined and interpreted. From the physical point of view, it means that colours emitted by two or more types of fluorescence molecules occupy the same pixel in the image. Biologically, colocalization means the attachment of two or more different molecules to the same structure in the cell. In the context of digital imaging, it can be described as the spatial overlap of two or more dyes in a multichannel image. Colocalization is usually presented as a plate consisting of three separate images: first two images show fluorescence according to two different channels, while the third one, combining two channels into a single image, is used to reveal overlapping/colocalized pixels.

1.2. Importance of colocalization observations

Recent years see a steady growth of publications employing colocalization experiments and citing colocalization observations. It is likely due to the improved quality and accessibility of confocal microscopes in research laboratories worldwide, and hence more researchers can obtain and meaningfully interpret the results of their colocalization experiments. Importance of colocalization observations can be summarized as follows:

(a) colocalization observations are strongly present in contemporary cell and molecular publications; number of articles describing colocalization is constantly growing;
(b) finding of colocalization is frequently indispensable in identifying the exact location of the structures of interest, therefore lending support for their common structural and functional characteristics;
(c) when estimated quantitatively, colocalization is capable of providing an important new information, e.g. to characterize the changes of the location of studied structures in dynamics and describe a selective contribution to observed colocalization of each of the studied molecule.

It should be mentioned that some studies tend to misinterpret colocalization observations by assigning functional characteristics to detected colocalized molecules (North, 2006). It needs to be stressed that a mere observation of colocalization does not provide such proofs. It does, however, assist in unifying the results of structural and functional experiments and thus frequently represents a required piece of decisive information.

1.3. Tools to detect colocalization

It is commonly agreed that reliability of colocalization experiments directly depends on the quality of analyzed images (Costes et al., 2004; Manders et al., 1992, 1993). That is why only images produced by confocal microscopes have sufficient quality suitable for quantification. In addition, estimation of colocalization relies on

specialized algorithms implemented in computer software. The best software packages appear to be not the ones bundled with the microscopes, but stand-alone applications developed specifically for the purpose of analyzing colocalization. As a rule, these applications are more feature-rich, thoughtfully designed, and frequently updated to be useable with the latest versions of computers system software, either for Windows or Macintosh platforms. As a main requirement to these software applications, they should provide full compatibility with image files generated by various brands of confocal microscopes and ensure preservation of digital image properties required for calculation process. Thus, the tools to detect colocalization can be divided as follows:

(a) cell and molecular biological tools needed to prepare samples to be used for colocalization observations;
(b) image acquiring tools, such as confocal microscopes;
(c) specialized computer software packages to be employed for quantification of the images with colocalization.

2. Overview of the quantitative colocalization analysis method

The method of quantitative colocalization analysis starts from simple counting of the pixels believed to represent colocalization and then compares their number with the total number of pixels in the image using various graphics-editing software applications, like Adobe Photoshop, GraphicConverter, etc. For example, if the molecules of interest were visualized using corresponding red- and green-labeled secondary antibodies and eventually counted according to the red–green channel pair, estimation of overlapped/colocalized yellow was considered to be a measure of colocalization. Although this approach is unfortunately still used in some studies, it very soon became clear that it is way too primitive and produces wrong results, because it ignores pixels with colour components (Manders et al., 1993). In addition, it was also shown that careless processing of confocal images with colocalization in graphics-editing software can irreversibly destroy the image data properties needed for quantification (Adler et al., 2008). Thus, several specialized algorithms were either adopted or introduced specifically to perform quantification of observed colocalization and understand its significance (Manders et al., 1993). In this section, we describe the method of quantitative colocalization in detail focusing on the rules of acquisition of images, their preparation for quantification, and interpretation of the obtained results.

2.1. Steps of quantitative colocalization analysis

Quantitative colocalization analysis can be divided in several steps, such as: (1) image acquisition, (2) background correction, (3) coefficients calculations, and,

Table 1. Steps of quantitative colocalization analysis.

Step of analysis	Brief description
1. Image acquisition	Images should be obtained using sequential scanning for each channel to eliminate the "cross-talk" of chromophores and to ensure the reliable quantification of colocalization and saved in tagged image file format (TIFF) format to prevent loss of information
2. Background correction	A. The extent of background correction depends on a variety of factors, including the intensity of immunofluorescence and the models of microscopes used to acquire images B. For the results to be comparable, background correction settings should be the same for all images in a study
3. Coefficients calculations	Several algorithms, such as Pearson's correlation coefficient (PCC), overlap coefficient according to Manders (MOC), overlap coefficients k_1 and k_2, colocalization coefficients m_1 and m_2, and colocalization coefficients M_1 and M_2, use different approaches to estimate colocalization and have different sensitivity and applicability What coefficient to use depends on the images to be examined. In majority of cases, PCC provides clear and applicable results If one antigen is stained stronger than another, then MOC should be employed, as it allows to quantify colocalization coefficients in these images more reliably
4. Interpretation of obtained results	A. PCC – correlation of the intensity distribution between channels B. MOC – the true degree of colocalization C. Overlap and colocalization coefficients – contribution of each particular antigen to the areas with colocalization

finally, (4) interpretation of the obtained results. These steps and their brief description are summarized in a table (Table 1).

2.2. Guidelines for examining images with colocalization

Reliable and interpretable analysis of confocal images with colocalization can only be made if certain rules of sample preparation, microscope set-up, as well as image acquisition and handling, were followed. Ignoring them will inevitably result in obtaining images unusable for quantification purposes. These rules are as follows:

(1) Sample preparation:

(a) Choose antibodies that are clearly antigen specific and do not cross-react.
(b) Ensure that selected secondary antibodies have well-separated emission and excitation spectra.
(c) Do not change mounting medium for the samples to be compared.
(d) Use cover glass of the same thickness for the samples to be compared.

(e) Try to examine only freshly stained samples, if there is need to re-examine samples, try avoiding anti-fading reagents, as their use can increase background fluorescence.
(f) Always check for autofluorescence using controls samples that were left unstained.

(2) Microscope set-up:

(a) For reducing chromatic shift, use plan apochromatic lenses.
(b) For maximizing emission collection and avoiding bleed-through effect, use optimized emission filters.
(c) Use the same objective lens for the samples to be compared.
(d) Ensure that the size of microscope pinhole during image collection is constant and properly set.

(3) Image acquisition and handling:

(a) For minimizing bleed-through effect, acquire images exclusively by sequential scanning.
(b) For preventing saturation, do not acquire too bright and too contrast images.
(c) Never manipulate obtained images in graphics-editing programs, as they alter the digital profile of images and eventually may ruin their usability for quantification.
(d) If you need to re-save image files, do it exclusively in lossless TIFF format.

2.3. Coefficients used to estimate colocalization

Colocalization can be estimated by calculating a number of values representing the proportion of colocalized pixels. These values are called colocalization coefficients. The most important of them and their usage have been recently reviewed (Zinchuk et al., 2007b). We compiled a table that includes information about coefficients with their meanings, values, and information on how they should be utilized (Table 2).

2.4. Background correction as a crucial step in quantifying colocalization

As we stated above, quality of images is the key to obtaining reliable calculations results. That is why images produced by conventional fluorescence microscopes are usually not suitable for quantification. However, even confocal images should not be used for quantification without adjustments, because they contain a certain amount of out-of-focus light coming from adjacent scanned planes. This problem is manifested by the presence of background noise (pixels of ''uncertain'' values), which is especially ominous when analyzed images are of low contrast and/or have weak fluorescence. If not removed, pixels of these values may interfere with the execution of implemented coefficients algorithms and cause erroneous coefficients readings. It was reported that the use of unadjusted images may result in up to 30% overestimation of colocalization (Landmann and Marbet, 2004).

Table 2. Summary of information about coefficients used to quantify colocalization with meanings, values, and information of how they can be utilized.

Coefficient	Meaning	Values	Use
Pearson's correlation coefficient (Rr)	Describes the correlation of the intensity distribution between channels	Ranges from −1.0 to 1.0; 0 indicates no significant correlation and −1.0 indicates complete negative correlation	Useable in any colocalization experiment
Manders' overlap coefficient (R)	Indicates an actual overlap of the signals, is considered to represent the true degree of colocalization	From 0 to 1.0; 0.4 implies that 40% of both selected channels colocalize	Can be used in any colocalization experiment, especially applicable when the intensities of fluorescence of detected antigens differ
Overlap coefficients k_1 and k_2	Split the value of colocalization into the two separate parameters, allows to determine the contribution of each antigen to the areas with colocalization	Vary	Useable in any colocalization experiment
Colocalization coefficients m_1 and m_2	Describe the contribution of each one from two selected channels to the pixels of interest	From 0 to 1.0; m_1 and m_2 of 1.0 and 0.3 for red–green pair imply that all red pixels colocalize with green, but only 30% of green pixels colocalize with red	Useable in any colocalization experiment
Colocalization coefficients M_1 and M_2	Identical to m_1 and m_2, but applied to analyzing Scatter Gram ROI	From 0 to 1.0; M_1 and M_2 of 1.0 and 0.3 for red–green pair imply that all red pixels colocalize with green, but only 30% of green pixels colocalize with red	Useable in any colocalization experiment

Several tools, such as filtering, deconvolution, and background correction were used with varying degrees of success to circumvent this problem by improving the quality of images prior to colocalization analysis (Shaw and Rawlins, 1991; Demandolx et al., 1997; Zinchuk et al., 2007a, b). While these tools have both their

advantages and limitations (see below), it should first of all be stressed that unadjusted images should never be used for quantification of colocalization. In fact, the latest software applications even adopt image correction as a default and standard procedure in quantification of colocalization (Zinchuk et al., 2004, 2005, 2007a, b; Fujii et al., 2009). However, a considerable number of articles that use ''raw'' (unadjusted) confocal images for analysis continues to be published, thus not only rising serious concerns about accuracy of the reported quantitative colocalization observations themselves, but also preventing the use of them for comparison purposes.

Among mentioned image correction tools, filtering is easy to apply, but its drawback is that filtering can result in introduction of image artifacts leading to false-positive coefficients readings (Landmann and Marbet, 2004). Another tool, deconvolution, aims to improve images by correcting diffraction-induced distortions and produces images that exceed diffraction-limited resolution. While some researchers praised deconvolution (Landmann and Marbet, 2004, Sedarat et al., 2004), others concluded that it has no effect on estimation of colocalization and is irrelevant (Nakamura et al., 2007). Concern was also expressed that deconvolution results in too drastic transformation of analyzed images and it is therefore questionable whether these deconvoluted images can in fact accurately represent the real nature of underlying biological processes.

Good results were reported using a procedure that removes pixels of selected background values, i.e. corrects background based on algorithms applied for the most common types of confocal fluorescence microscopy images. Specialized software background correction tools give the options to correct background in either auto or manual mode (Fig. 1). In auto mode, background can be conveniently corrected for the most common images types: (a) average contrast and fluorescence, (b) low contrast, and (c) weak fluorescence (Fig. 1a). After the image pattern is chosen, software will rely on specialized algorithms to subtract the pixels of selected values from the image. In addition, it is also possible to correct background by selecting the actual background on images and let algorithms subtract that pixel information too (Fig. 1b). Also, if necessary, one can use a simple threshold and choose the desired values of pixels to be removed from the image (Fig. 1c).

Fig. 2 shows images before and after background correction and is accompanied by their respective scatter grams. Fig. 2a presents image with non-corrected background and its scatter gram (Fig. 2a′). Fig. 2b shows image with background corrected in auto mode. As it can be seen on scatter gram, this mode may be too rough for the image, because it removes an excessive amount of background pixel values (Fig. 2b′). Fig. 2c presents image with background corrected using a selected region of interest (ROI), the procedure indicated by an arrow on Fig. 2a. Fig. 2c′ shows representation of its respective scatter gram. The extent of removed pixel values (black areas along X and Y axes) is relatively low and thus acceptable. Colocalized pixels are located along the diagonal of scatter gram. Importantly, selecting similar areas in different regions of image background results in almost identical representation of scatter grams, indicating consistency and usability of this approach.

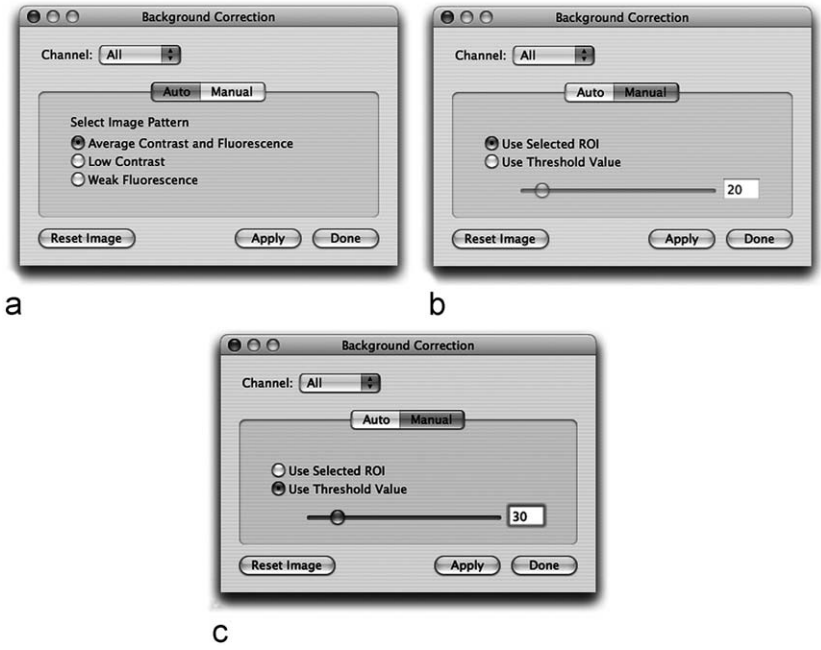

Fig. 1. Options for background correction (based on characteristics of the most common image types in auto (a) and manual mode using selected ROI (b) and threshold values (c).

It was recently reported that image background can be corrected using the information contained in the temporal dynamics of its individual pixels (Chen et al., 2006). Importantly, according to its description, it can be used regardless of the staining profile in the surrounding tissue. This approach offers background correction for homogenous and non-homogenous backgrounds and claims to be able to deal with background inhomogeneities within a single ROI. Its disadvantage is that it needs dynamics and cannot be applied to still images, which makes it still unusable for the majority of images used in quantitative studies.

Another recent report described an approach based on replicate-based correction correlation to be used for background correction (Adler et al., 2008). Unfortunately, it requires two images for each channel (four in total) to perform background correction, which makes it difficult for researchers accustomed to take either two of them or just a single merged image to analyze already acquired images from their data bases. Besides, in disagreement with the results of studies that used image adjustments tools described above, the study that reported the replicate-based correction correlation surprisingly found higher numbers of coefficients following its use compared to the intact images. Therefore, while interesting, the mentioned approach requires further testing and improvements before it can be recommended to researchers for adoption.

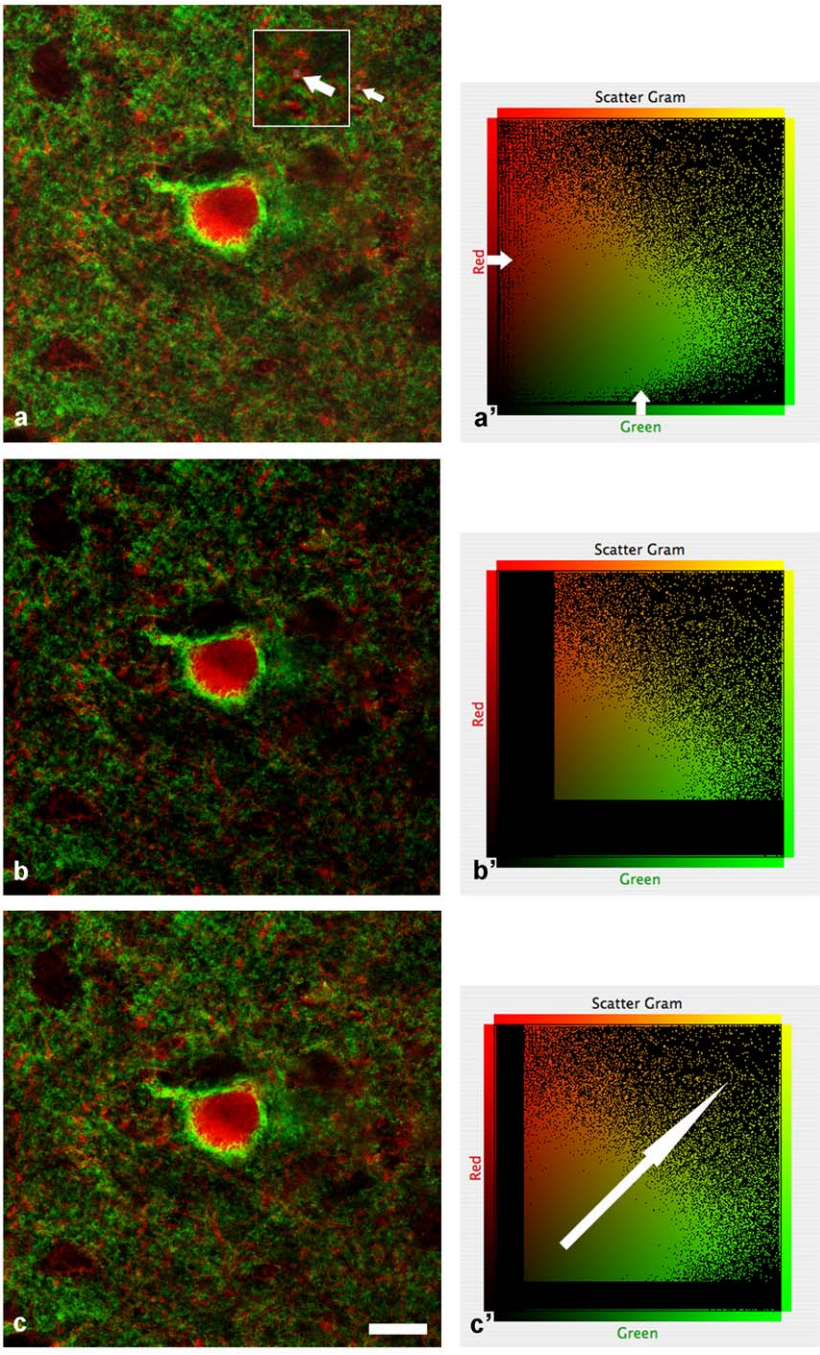
a
Scatter Gram
Red
Green
a'
b
Scatter Gram
Red
Green
b'
c
Scatter Gram
Red
Green
c'

2.5. Cross-talk and the ways to minimize it

Cross-talk is a frequently encountered issue in multicolour confocal imaging which can significantly impair the reliability of quantitative colocalization calculations. It occurs because of the interaction between emission and excitation spectra of the used fluorophores. Cross-talk can be further categorized as: (a) cross-emission, (b) cross-excitation, and (c) undesired fluorescence resonance energy transfer (FRET) (Kong et al., 1999; Lakowicz, 2006).

In the case of cross-emission, also known as emission bleed through, overlapping of emission spectra of two fluorophores will result in extension of emission from one channel into another and eventually produce false-positive colocalization. This is a common problem because of the overlapping spectra of some popular fluorophores, such as, for example, fluorescein iso-thiocyanate (FITC) and tetramethyl rhodamine iso-thiocyanate (TRITC), FITC and 4′,6-diamidino-2-phenylindole (DAPI). That is why it is advisable to use single-stained control specimens in any colocalization experiments. The problem of emission bleed through can be remedied by selecting fluorophores that do not overlap and using a sequential scanning mode. In this mode, using single excitation at a time and collecting a wider range is safe, because there is no emission coming from a second channel.

Another cross-talk issue, cross-excitation, occurs due to the tendency of some fluorophores (for example FITC and TRITC) to produce excitation at other wave lengths than their peaks as well, which can interfere with the peak excitations of other fluorophores. Cross-excitation itself does produce false-positive colocalization, but it can contribute to false-positive colocalization created by cross-emission.

Undesired FRET occurs when emission spectrum of one fluorophore falls within the close vicinity (1–10 nm) of excitation spectrum of another fluorophore. In this case, the emission energy of the first fluorophore will be transferred to the second fluorophore and it will act as excitation energy. As a result, the first emission intensity will be reduced, while the second will be increased. Examples of these

Fig. 2. A panel of confocal images of a cortical parvalbumin-expressing neuron (red) double stained for spectrin (green) with no background correction (a) and with background corrected in auto (b) and manual mode using selected ROI (c). Respective scatter grams of the images are shown below (a′, b′, c′). Area used for selecting pixel values for background correction using area selection is indicated by an arrow and magnified (a). Note that images b and c appear darker due to removal of pixels of the fixed and selected values. Scatter gram a′, representing image without corrected background, shows widely dissipated green and red pixels along *X* and *Y* axes. Background correction in auto mode for this image removed too many pixels, including those which may have represented colocalization (b′). Background correction in manual mode using selected ROI removes less pixels, preserving yellow, colocalized pixels, which tend to concentrate along the diagonal of the scatter gram (c′). Three images from three sections were examined. Representative image is shown. The scale bar indicates 20 μm (applicable to images a–c). (For interpretation of the references to color in this figure legend, the reader is referred to the web version of this article)

fluorophores pairs can be FITC and TRITC, yellow fluorescent protein (YFP) and green fluorescent protein (GFP). This phenomenon may result in either false-positive, false-negative colocalization, or both. As with cross-emission, the best way to exclude undesired FRET is to use fluorophores with distinctively different excitation and emission spectra.

2.6. Impact of ROI selection

Selection of region of interest is an important step of quantitative colocalization analysis. ROI defines a portion of image that contains areas with colocalization. Accuracy of calculations can be improved by minimizing the number of pixels surrounding the areas with colocalization to be included into the count. Fig. 3 and respective Table 3 show the results of coefficients calculations on the same image and for the same area with colocalization, but using two popular ROI types, such as rectangle (Fig. 3a) and lasso (Fig. 3b). Lasso ROI selection includes predominantly pixels with colocalization and therefore produces more accurate coefficients results compared to rectangle ROI (Table 3). Importantly, discrepancies between calculations using different ROI selections directly depend on the quality of analyzed images. Properly acquired images with corrected background are significantly less susceptible to the differences of ROI selection. In the majority of cases, like in the one shown, the discrepancies of calculations obtained using different ROI types are minor and do not interfere with the conclusions about either presence or absence of colocalization (see Table 5). It should be remembered, however, that the exact pixel size of selected ROIs is crucial for the purpose of comparing the results of colocalization coefficients calculations between different experiments in the same study as well as with other studies, i.e. perfect comparison of the results of colocalization coefficients calculations requires use of images of the same pixel size and resolution.

2.7. Revealing colocalized pixels

In addition to calculation of colocalization coefficients, it is frequently equally important to determine the exact locations of the areas with colocalization. Tools of quantitative colocalization analysis software visually empower the quantitative assessment of colocalization by providing the ability to view the locations of actually colocalized pixels on examined images. Fig. 4a shows colocalization (yellow areas) of spectrin (red fluorescence) and restrictin (green fluorescence) molecules in the rat cortical neurons. With the help of specialized algorithms, it is possible to determine the locations of actually colocalized pixels on them (white areas) (Fig. 4b). The distribution of these pixels clearly demonstrates that colocalization should not be evaluated by the naked eye alone, as the actual appearance of them on Fig. 4b differs from the appearance one may expect when looking at Fig. 4a.

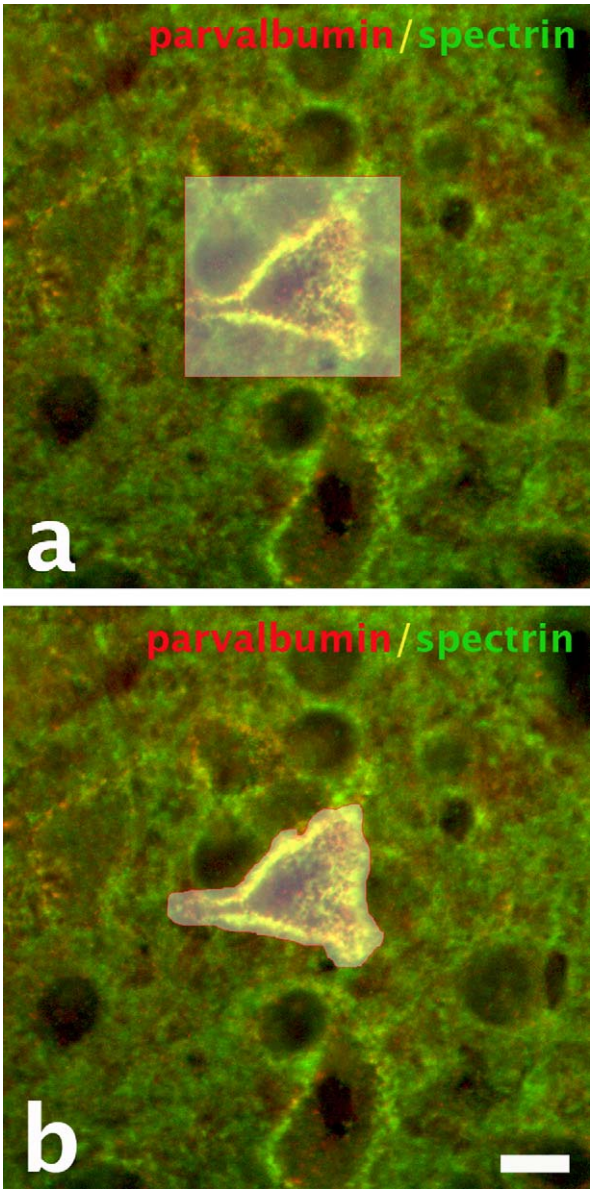

Fig. 3. An example of using different ROI types to select areas with colocalization. Image of a cortical parvalbumin-expressing neuron (red) double stained for spectrin (green) is shown. Rectangle ROI selection (a) includes more pixels to the count and eventually results in slightly lower coefficients numbers compared to the lasso ROI selection (b) (Table 3). If less surrounding colocalization pixels are included into the count, more accurate results will be obtained. Three images from three sections were examined. Representative image is shown. Scale bar indicates 20 μm and applicable to both images. (For interpretation of the references to color in this figure legend, the reader is referred to the web version of this article.)

Table 3. Comparison of the results of coefficients calculations using selections of different ROI types.

Coefficient	Rectangle ROI	Lasso ROI
Pearson's correlation coefficient (Rr)	0.7974 ± 0.08	0.8268 ± 0.10
Manders' overlap coefficient (R)	0.9634 ± 0.11	0.9699 ± 0.09
Overlap coefficients k_1 and k_2	0.9843 ± 0.09 and 0.9430 ± 0.09	0.9166 ± 0.10 and 1.0263 ± 0.10
Colocalization coefficients m_1 and m_2	0.9937 ± 0.11 and 0.9992 ± 0.12	0.9906 ± 0.08 and 0.9999 ± 0.09

Note that the use of lasso ROI results in slightly higher numbers of calculated coefficients. Statistical comparisons were performed using the Mann–Whitney U test. An average of coefficients of three examined images is shown. $P < 0.05$.

2.8. A quantitative colocalization analysis protocol

We summarized steps required to successfully perform colocalization analysis in a protocol. The protocol is divided in four parts: (1) tissue preparation, (2) immunofluorescence staining, (3) microscopy, and (4) image analysis (Table 4). As an example, it describes quantification of colocalization of parvalbumin and spectrin molecules in cortical parvalbumin-positive neurons of the rat.

2.9. Interpretation of obtained results

Interpretation of the results of coefficients calculations concludes the quantitative colocalization analysis protocol and is crucially important, because the vast majority of calculations falls within the range of values indicating neither complete presence nor complete absence of colocalization. Based on the results of thousands of analyzed images from different tissues, microscopes, and laboratories worldwide, it was possible to compile a table with interpretation of coefficients results (Zinchuk and Zinchuk, 2008). The table should be viewed as a guide that assists in understanding and comparing the results of calculations. As can be seen from the table, five different types of coefficients do not show exactly the same trends in how their values can be understood, thus require an individual approach in their interpretation (Table 5).

To summarize information presented above, we created a flow chart showing a complete experimental procedure for quantitative colocalization analysis (Fig. 6).

2.10. Troubleshooting colocalization

Protocol presented above is focused on important rules that should be followed when preparing samples with colocalization and observing them in confocal

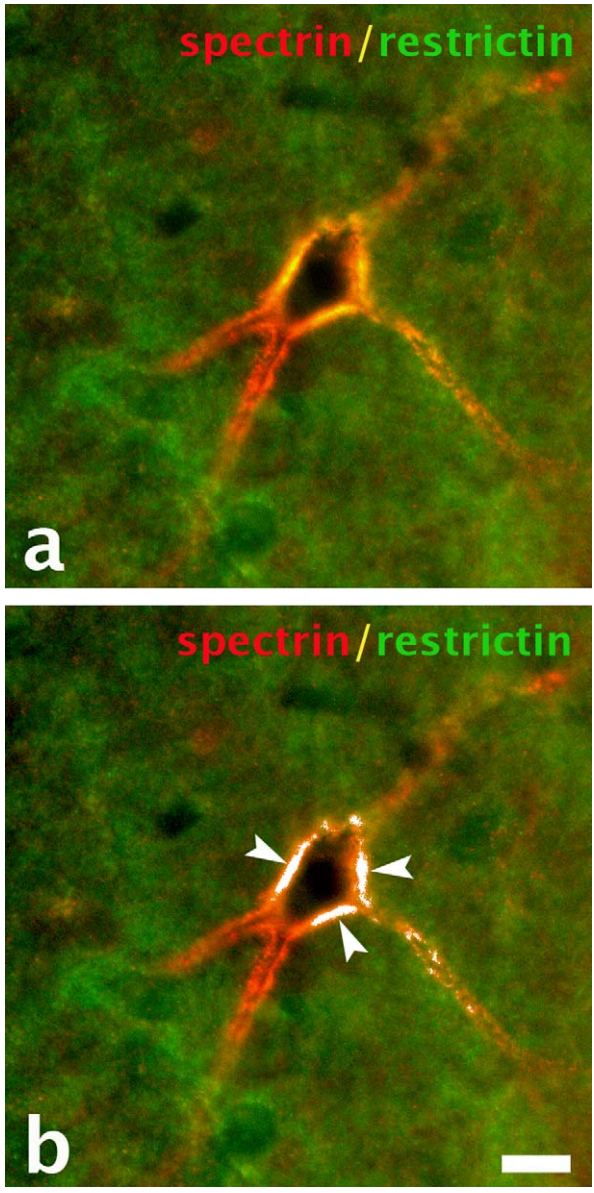

Fig. 4. Actually colocalized pixels revealed on their original image location. Image (a) shows colocalization of spectrin and restrictin in rat cortical neurons. Image (b) shows areas where they are actually colocalized in white color as indicated by arrowheads. Note that areas with actual colocalization appear to be rather smaller than expected. Scale bar indicates 20 μm and equally applicable to both images.

Table 4. A quantitative colocalization analysis protocol.

1. *Tissue preparation*
   1. Anesthetize a rat with CO_2
   2. Open chest with sharp scissors and transcardially perfuse it with 0.1 M PBS, followed by an ice-cold 4% 0.1 M phosphate-buffered paraformaldehyde
   3. Gently excise brain and postfix it in 4% 0.1 M phosphate-buffered paraformaldehyde in refrigerator at 4 °C overnight
   4. Transfer brain to 30% sucrose for 2 days
   5. Place tissue in the cryostat chamber and allow the temperature in it to equilibrate with the temperature of brain
   6. Cut 8–10 μm thick cryosections, pick them up on glass slides, and air dry. It is best to use cut sections for staining right after cutting; if necessary sections can be stored for up to 2 weeks at −20 °C
2. *Immunofluorescence staining*
   1. Mark an area on a glass around tissue with a water repellent marker, apply blocking solution inside of it, and incubate for 60 min. The section should be kept wet during the entire procedure
   2. Discard the blocking solution
   3. Apply solution of primary antibody A (in this protocol anti-parvalbumin antibody), dilute 1:500, and incubate for 60 min
   4. Rinse with 0.1 M Tris-buffered saline (TBS) (three times for 5 min)
   5. Apply solution of primary antibody B (anti-spectrin in example 1 and anti-restrictin in example 2), dilute 1:500 and 1:1000, respectively, and incubate for 60 min
   6. Rinse with 0.1 M TBS (three times for 5 min)
   7. Apply mixture of corresponding secondary antibodies (Alexa 568 and Alexa 488), dilute each 1:400, and incubate for 1 h in the dark
   8. Rinse with 0.1 M TBS (three times for 5 min with gentle agitation)
   9. Mount sections with glycerine and coverglass
   10. In parallel, perform the same procedure using normal serum for control of the specificity of immunostaining. Sections should be examined in microscope immediately after staining
3. *Microscopy*
   1. Use immersion lens of microscope to view sections
   2. Make sure that sections are negative for autofluorescence. If any signs of autofluorescence are detected, discard sections. If not, continue viewing them
   3. Visualize double fluorescence for red and green channels using an argon–krypton laser at wave lengths 543 and 488 nm, respectively
   4. Once optimized, do not modify position of the pinhole of the microscope to ensure that images are comparable
   5. After detecting areas with colocalization, try to select those which are not too bright and not too contrast
   6. Perform sequential scanning for each channel to minimize the cross-talk of fluorophores
   7. Save either a merged (containing both channels) image file or two separate channels image files. In the latter case, use merge tool of the software to merge them in one before performing calculations. Make sure the files are saved with maximum possible pixel size and image resolution and in the lossless (TIFF) format. Ensure that image background is properly balanced, i.e. neither too bright nor completely dark
4. *Image analysis*

Table 4. (*continued*)

Image analysis can de divided into 3 steps: (A) background correction, (B) calculation of colocalization coefficients, and (C) viewing colocalized pixels

A. Background correction

Background can be corrected either in auto (a) or manual mode (b and c)

1. Use either local network of your institution or removable media to transfer images from confocal microscope to a computer for analysis. We use an Intel Mac Pro running Mac OS X 10.5, but even significantly older PowerPC-based Macs should satisfy your needs
2. Start up CoLocalizer Pro software and drag-and-drop the image you will be analyzing to the application main window
3. Perform background correction on the imported image. Image should not be processed for coefficients calculations if background was left uncorrected. The software will issue a warning if user attempts to perform coefficients calculations without background correction. It is important to remember that background correction will impact results of all coefficients calculations. Poorly corrected background will result in wrong results of coefficients calculations
4. Select background correction settings applicable to your image. If unsure, start with auto mode. Results of background correction should be assessed by examining the image scatter gram. It is needed to clarify the results of background correction, because visual appearance of images after background correction is not always informative

(a) *Correcting background in auto mode*

(i) Click ''Background'' icon in the application tool bar or choose ''Background Correction'' under the ''Tools'' in the application menu bar

(ii) In the opened ''Background Correction'' window, select ''All'' channels (Fig. 1a)

(iii) Under the ''Auto'' tab, select the pattern of the image closest to the one being analyzed among the followings: (a) ''Average Contrast and Fluorescence'', (b) ''Low Contrast'', and (c) ''Weak Fluorescence'' and click ''Apply''. The ''Average Contrast and Fluorescence'' option should be optimum in the majority of cases. Depending on the images, the ''Low Contrast'' and ''Weak Fluorescence'' options may be too rough and remove too many pixels data

(iv) Dismiss ''Background Correction'' window by clicking ''Done''. As a result, image in the main window will appear slightly changed (darkened) due to removal of the portion of pixels (Fig. 2b, c)

(v) Following this correction, examine image scatter gram. Fig. 2a′ shows scatter gram of the intact image. Excessive background correction will result in scatter gram similar to the one shown on Fig. 2b′. In this case, background correction will need to be repeated using different settings, such as correction in manual mode using selected ROI. First, reset image by selecting ''View'' in the application menu bar and then choose ''Restore to Original''. It is advised to reset image every time a different background correction mode is chosen

(b) *Correcting background in manual mode using selected ROI*

This method is superior to any other currently used method of background correction, because it allows to adjust it to the unique pixel profile of the analyzed image:

(i) Click ''Background'' icon in the application tool bar or choose ''Background Correction'' under the ''Tools'' in the application menu bar

(ii) In the opened ''Background Correction'' window, select ''All'' channels (Fig. 2b)

(iii) Under the ''Manual'' tab, click ''Use Selected ROI'' radio button

Table 4. (*continued*)

(iv) Using either "Rectangular" or "Oval" ROI selection tool (accessible from "ROI" in the application menu bar), select a small area of approximately 10×10 pixel size in the image background. When examining tissue sections, this area should be selected in the tissue background which is dark, but not completely black, i.e. absorb some fluorescence (Fig. 2a). Pixel levels within such areas can be considered as the ones representing background. When examining cells in culture, select similarly small area outside the cells. Then, click "Apply" and dismiss "Background Correction" window by clicking "Done"

(v) Following this correction, examine image Scatter Gram. Fig. 2c′ shows Scatter Gram of the image with properly corrected background. Successful background correction will show pixels concentrating along the diagonal of the Scatter Gram, while the majority of pixels from left and bottom will be removed. The areas of the removed pixels should be not too wide

(c) *Correcting background in manual mode using threshold value*

In some cases correction in manual mode using selected ROI may not produce expected results. In addition, images may not fall in any of the suggested categories of auto mode being too bright and/or too contrast than the average images. In these cases, background can be corrected using threshold value, when it is possible to exactly specify the exact number of the pixels to be removed. If any of above-described methods of correction was used prior to this, reset image by selecting "View" from the application menu bar and then choose "Restore to Original". Then:

(i) Click "Background" icon in the application tool bar or choose "Background Correction" under the "Tools" in the application menu bar

(ii) In the opened "Background Correction" window, select "All" channels (Fig. 1c)

(iii) Under the "Manual" tab, click "Use Threshold Value" radio button. This activates slider to select the number of pixels to remove. Choose somewhere between 20 and 40, this should produce the best results. Then, click "Apply" and dismiss "Background Correction" window by clicking "Done". Examine Scatter Gram before proceeding to calculation of coefficients. It should look similar to the one shown on Fig. 2c′. Once determined, background correction settings should be used consistently for all images to be compared

B. Calculation of colocalization coefficients

Coefficients can be calculated using either the whole image as a ROI or by selecting areas with colocalization and performing calculations exclusively on them. When whole image is used as a ROI, calculations are easier to compare and reproduce. If coefficients are calculated on selected areas, the results are usually more precise

Using whole image as a ROI

(i) With colocalization window opened and whole image previewed, select a pair of channels according to which coefficients should be calculated, for example red–green (Fig. 5b). Pixel Information section of the window will display its pixel count

(ii) Select coefficients to be calculated. Calculate as many as possible

(iii) After calculating coefficients on image ROI, click Scatter Gram ROI tab (Fig. 5f) and calculate M_1–M_2 coefficients for Scatter Gram ROI

(iv) Export calculation results as Text or Excel files to be analyzed statistically

(v) Prepare reports of the session in HTML and/or PDF format. Save not only coefficients results, but also image data. Include Scatter Gram in the analyzed image to be used for presentation

(vi) Evaluate calculated results statistically, make sure the results are significant

Table 4. (*continued*)

Using ROI selection tools

(i) Using ROI selection tools (accessible from "ROI" in the application menu bar), select the tool which will allow the most precise selection of the area to be analyzed (chose from "Rectangular", "Oval" "Polygon", and "Lasso"). The "Lasso" tool is the most accurate for selecting regions with irregular shapes
(ii) Select the area you would like to examine. Try to avoid pixels not belonging to it
(iii) Open colocalization window and select a pair of channels according to which coefficients should be calculated, for example red–green. Selected area will be displayed in the left bottom corner of the window (Fig. 5c)
(iv) Select coefficients to be calculated. Calculate as many as possible
(v) After calculating coefficients on image ROI, click Scatter Gram ROI tab (Fig. 5f) and calculate M_1–M_2 coefficients for Scatter Gram ROI
(vi) Export calculation results as Text or Excel files to be analyzed statistically
(vii) Prepare reports of the session in HTML and/or PDF format. Save not only coefficients data, but also images. Make sure to save the selected image ROI to be able to reproduce calculation results as precisely as possible, if needed. Include Scatter Gram in the analyzed image to be used for presentation
(viii) Evaluate calculated results statistically, make sure the results are significant

C. Viewing colocalized pixels

This methodological approach allows to trace the actually colocalized pixels in examined images to ensure that non-colocalized pixels are not misinterpreted as colocalized.

(i) After calculating coefficients, click "Reveal Pixels" tab of the colocalization window (Fig. 5g)
(ii) Under the opened tab, click "Colocalized" button to view actually colocalized pixels at their image location
(iii) To view pixels others than colocalized, select pixels of desired colour values on Scatter Gram (Fig. 5a). Use "Pixel Information" (Fig. 5d) to confirm them. Then, click "Selected" button to view them

The protocol is illustrated on quantifying colocalization of parvalbumin with spectrin and restrictin in the rat cortical parvalbumin-expressing neurons. Leica SP5 confocal microscope was used to acquire images. CoLocalizer Pro software was employed for background correction and coefficients calculations.

microscopes. However, there is still a number of issues that can potentially arise when performing this analysis. We summarized them in Table 6.

2.11. 2D versus 3D colocalization

Recently, a 3D approach was introduced for quantifying colocalization (Costes et al., 2004). 3D quantification can potentially be more accurate, because it performs calculations on volume reconstructed from images that contain less extra light originated from neighbouring scanned planes outside the plane of interest, thereby reduces the need for background correction. While the number of users of this approach is steadily growing, 2D approach is still the most commonly used and will likely remain the most relevant for a considerably long time.

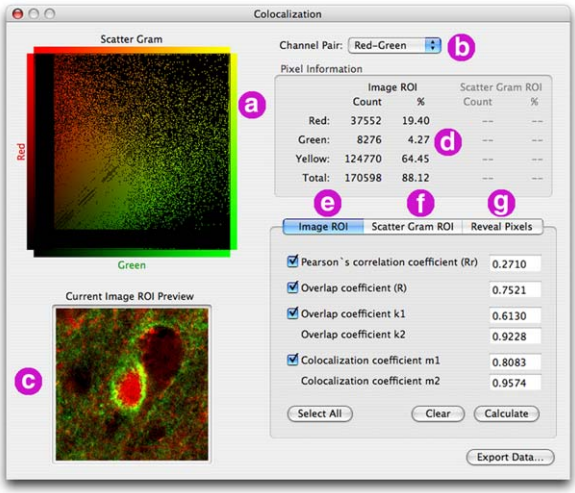

Fig. 5. Colocalization window of quantitative colocalization analysis software contains Scatter Gram of the selected ROI to be analyzed (either from the whole image like shown or selected area) (a), a pair of channels according to which colocalization will be examined (b), the ROI itself (c), and detailed pixel information about analyzed ROI (d). Under the tabs, options to calculate coefficients (e and f) and view selected and colocalized pixels (g) are also presented. After calculations are done, all results are exportable as Text and Excel files. All calculations data can be saved in HTML and PDF file formats as session reports.

Table 5. Interpretation of the results of coefficients calculations.

Coefficient	Standard values	Values indicating colocalization	Values indicating absence of colocalization
Pearson's correlation coefficient (Rr)	From −1.0 to 1.0	From 0.5 to 1.0	From −1.0 to 0.5
Manders' overlap coefficient (R)	From 0 to 1.0	From 0.6 to 1.0	From 0 to 0.6
Overlap coefficients k_1 and k_2	Vary	Close values (0.5 and 0.6, 0.8 and 0.9)	Distant values (0.5 and 0.9, 0.2 and 0.7)
Colocalization coefficients m_1 and m_2	Vary	Above 0.5	Below 0.5
Colocalization coefficients M_1 and M_2	Vary	Above 0.5	Below 0.5

Names of coefficients, their standard values, and values that should be interpreted as either presence or absence of colocalization are given. Results not falling within the range of standard values of coefficients reveal mistakes in sample preparation, microscope set-up, image acquisition and handling, and indicate that the used images are not suitable for quantification. Partially reproduced from Zinchuk and Zinchuk (2008) with permission from John Wiley & Sons, Inc.

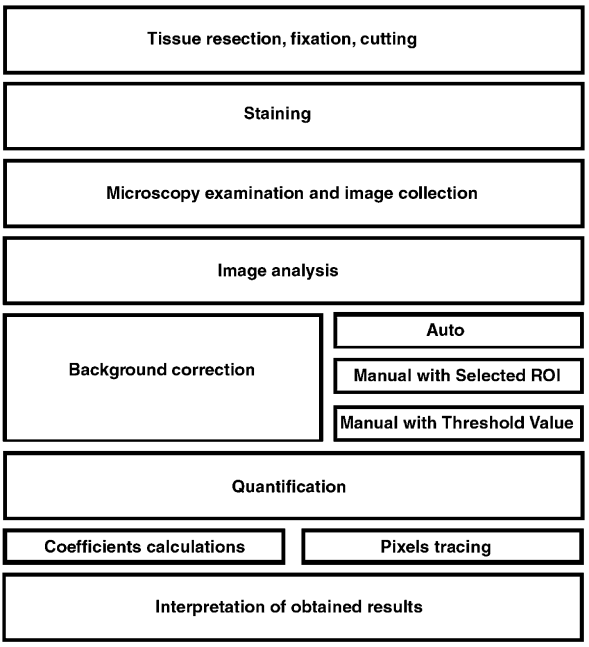

Fig. 6. A flow chart of the experimental procedure for quantitative colocalization analysis.

Table 6. Troubleshooting colocalization.

Step	Problem	Cause	Solution
Sample preparation	1. Strong background fluorescence	1.A. Poorly fixed tissue	1.A. Ensure that fixative is appropriate and fresh
		1.B. Tissue may have been stored for too long	1.B. Ensure that a recently collected tissue is used
		1.C. Sections may have dried during staining	1.C. Ensure that sections remain wet during staining
		1.D. Too high concentration of Triton X-100	1.D. Lower Triton X-100 concentration
		1.E. Suboptimal dilution of antibodies	1.E. Try other dilutions
		1.F. Wrong choice of the mounting medium	1.F. Try different mounting media or void using anti-fading reagents altogether; use glycerine instead

Table 6. (*continued*)

Step	Problem	Cause	Solution
Image acquisition and handling	1. Areas with colocalization look blurred	1.A. Images were acquired by simultaneous scanning	1.A. Acquire images exclusively by sequential scanning
		1.B. Microscope emission filters were not optimized	1.B. Ensure optimization of emission filters, i.e. use narrow band filters
	2. Images look saturated	2. Acquired images are too bright and/or too contrast	2. Avoid acquiring too bright and/or too contrast images
Quantification	1. Scatter Gram shows excessive number of pixels removed following background correction	1. Background was corrected excessively	1. If corrected in auto mode, switch to manual mode and try correction using selected ROI
	2. Scatter Gram shows insufficient number of removed pixels	2. Background was corrected insufficiently	2. If corrected using Selected ROI, select different ROI. If employing "Threshold Value", increase the number of to be removed pixels using slider
	3. Calculations results do not correspond to their pre-dedicated values	3. Flaw(s) in the image acquisition and handling (original image information may have been lost due to it has been saved not in TIFF format or edited)	3. Make sure to preserve original image information: do not resave it in any other format than TIFF, never manipulate images
	4. Unjustifiably big number of colocalized pixels shown when using "Colocalized" or "Reveal Pixels" tool	4.A. Image was acquired with either too dark or too bright background	4.A. Obtain another image with properly balanced background
		4.B. Suboptimal background correction	4.B. Repeat background correction using different settings

The possible problems, their causes and solutions are shown according to the steps of quantification analysis, such as "Sample preparation", "Image acquisition and handling", and "Quantification".

2.12. Triple colocalization

There is a growing interest to quantify colocalization of more than two molecules of interest, i.e. to perform quantification of triple or more colocalization (Mokin and Keifer, 2006). This simultaneous quantification can allow understanding more complex cell and molecular biological events. The possibility to use triple quantification of confocal images with colocalization was recently addressed in a study describing the use of a pixel-by-pixel algorithm (Goucher et al., 2005). The study reports presenting the degree of colocalization in percentage points and claims to be able to let users perform batch processing of analyzed images. The analysis is susceptible to the same problems of sample preparation, microscope set-up, and image acquisition and handling as described above for the two-channel analysis. It remains to be seen whether this approach will be used in other studies as well so that the results from different laboratories can be compared and used for understanding of their significance.

3. Examples of applications of quantitative colocalization analysis in neuroscience

In the examples below, we show how quantitative colocalization can be used and what practical lessons can be learnt from its applications.

3.1. Varying colocalization of extracellular matrix components in the perineuronal nets of cortical parvalbumin-expressing neurons

In the first example, we look at quantification of colocalization in the components of extracellular matrix in the perineuronal nets of cortical parvalbumin-expressing neurons (Grossenbacher-Zinchuk et al., 2008). The authors quantified colocalization using images of cortical parvalbumin-expressing neurons located in the layer V of temporal cortex in the rat that demonstrated colocalization with spectrin and restrictin.

Parvalbumin is a calcium-binding protein present in gamma-aminobutyric acid (GABA)ergic interneurons in the nervous system. It is expressed in chandelier and basket cells in the cerebral cortex. Spectrin and restrictin are extracellular matrix molecules associated with perineuronal nets surrounding parvalbumin-expressing neurons (Dityatev et al., 2007). Areas with colocalization were confined to surrounding neurons perineuronal nets. Visually, colocalization appeared not "prominent", but rather "moderate", thus rising a natural question about its degree (Fig. 7). Quantification was preformed using CoLocalizer Pro software (CoLocalization Research Software, Tokyo, Japan). The study determined PCC, an MOC, overlap coefficients k_1 and k_2, and colocalization coefficients m_1 and m_2. Background was corrected in manual mode using selected ROI.

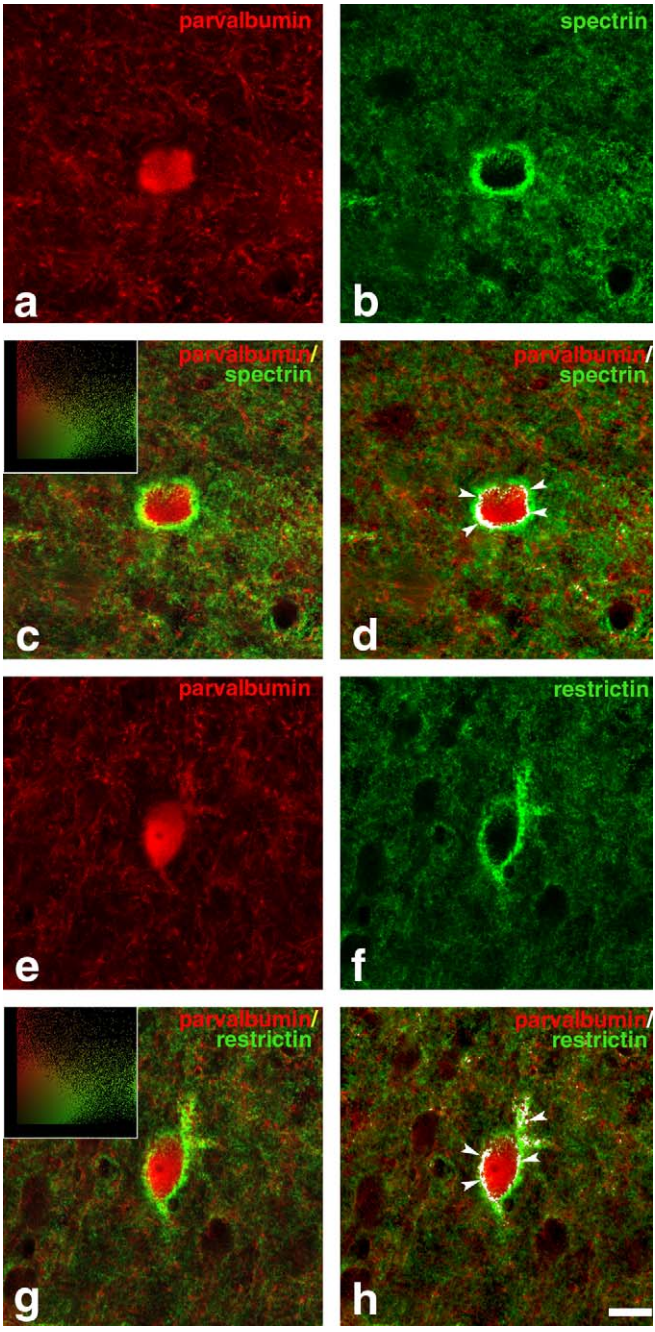
parvalbumin
a
spectrin
b
parvalbumin/
spectrin
c
parvalbumin/
spectrin
d
parvalbumin
e
restrictin
f
parvalbumin/
restrictin
g
parvalbumin/
restrictin
h

Table 7. Comparison of the values of coefficients obtained on images double stained for parvalbumin (red) and spectrin (green) calculated without background correction and with background corrected in auto (Average Contrast and Fluorescence preset) and manual (Selected ROI preset) modes.

Coefficient	Background not corrected	Background corrected in auto mode	Background corrected using Selected ROI
Pearson's correlation coefficient (Rr)	0.32 ± 0.05	0.27 ± 0.06	0.23 ± 0.04
Overlap coefficient according to Manders (R)	0.89 ± 0.11	0.84 ± 0.10	0.81 ± 0.05
Overlap coefficients k_1 and k_2	$k_1 = 0.64 \pm 0.10$ $k_2 = 0.96 \pm 0.06$	$k_1 = 0.82 \pm 0.08$ $k_2 = 0.84 \pm 0.10$	$k_1 = 0.81 \pm 0.10$ $k_2 = 0.82 \pm 0.09$
Colocalization coefficients m_1 and m_2	$m_1 = 0.97 \pm 0.04$ $m_2 = 1.00 \pm 0.06$	$m_1 = 0.93 \pm 0.04$ $m_2 = 0.96 \pm 0.06$	$m_1 = 0.91 \pm 0.05$ $m_2 = 0.95 \pm 0.08$

Calculation of coefficients with background intact results in 28% overestimation of colocalization (biggest change is observed for PCC (Rr), smallest for overlap coefficients k_1 and k_2). Statistical comparisons were performed using the Mann–Whitney U test. An average of coefficients of three examined images is shown. $P < 0.05$.

First, the authors showed dependency of the results of coefficients calculations on the background correction. As expected, background correction procedure influenced the results of coefficients calculations (Table 7 shows calculations for a parvalbumin–spectrin pair). Remarkably, comparison of coefficients values before and after background correction suggested that calculation of coefficients on images without background correction would have produced 28% and 9% of false-positive results (according to PCC and MOC, respectively). This observation is in agreement with other studies (Landmann and Marbet, 2004; Zinchuk et al., 2007b). Importantly, such overestimation of colocalization may have produced erroneous

Fig. 7. A panel of images showing colocalization of parvalbumin with spectrin (a–d) (upper row) and restrictin (e–h) (lower row) in the rat cortical parvalbumin-expressing neurons. Representative images are shown. Parvalbumin (red) (images a and e) was detected using anti-parvalbumin antibody. Spectrin (green) (image b) and restrictin (green) (image f) were detected using anti-spectrin and anti-restrictin antibodies, respectively. Alexa 594-labeled secondary antibody was used to visualize parvalbumin fluorescence and Alexa 488-labeled secondary antibody was used to visualize spectrin and restrictin fluorescence. Parvalbumin-expressing neurons show immunostaining of their soma (a and e), while both spectrin and restrictin are detected around it. Figures c and g, accompanied by their respective scatter grams, show yellowish regions suggesting colocalization. Precise areas with colocalization, revealed in white color (arrowheads), appear in punctuated and uneven fashion around soma of neurons (d and h). Results of calculations on images with colocalization (c and g) are shown in Table 7. The scale bar indicates 20 μm (equally applicable to all images). (For interpretation of the references to color in this figure legend, the reader is referred to the web version of this article.)

Table 8. Values of coefficients calculated on images with parvalbumin–spectrin and parvalbumin–restrictin colocalization shown in Fig. 7.

Coefficient	Parvalbumin–spectrin colocalization	Parvalbumin–restrictin colocalization
Pearson's correlation coefficient (Rr)	0.23 ± 0.04	0.20 ± 0.04
Overlap coefficient according to Manders (R)	0.81 ± 0.05	0.75 ± 0.08
Overlap coefficients k_1 and k_2	$k_1 = 0.81 \pm 0.1$ $k_2 = 0.82 \pm 0.09$	$k_1 = 0.70 \pm 0.06$ $k_2 = 0.83 \pm 0.09$
Colocalization coefficients m_1 and m_2	$m_1 = 0.91 \pm 0.05$ $m_2 = 0.95 \pm 0.08$	$m_1 = 0.83 \pm 0.10$ $m_2 = 0.92 \pm 0.08$

Three images from three sections were quantified. Background was corrected in manual mode using Selected ROI. Statistical comparisons were performed using the Mann–Whitney U test. A $P < 0.05$ was considered to be statistically significant.

conclusions about its degree and even resulted in interpreting it as presence when in fact it should be regarded as absence.

Calculations on images with corrected background showed that MOC values are within the range of those indicating colocalization (0.81 for a parvalbumin–spectrin pair and 0.75 for a parvalbumin–restrictin pair), while PCC indicated numbers which should be interpreted as its absence (0.23 for a parvalbumin–spectrin pair and 0.20 for a parvalbumin–restrictin pair). It was, therefore, necessary to consider other coefficients, such as pairs of k_1–k_2 and m_1–m_2 coefficients. These two pairs of coefficients showed values clearly indicating colocalization (k_1–k_2 were 0.81–0.82 and 0.70–0.83 and m_1–m_2 were 0.91–0.95 and 0.83–0.92 for parvalbumin–spectrin and parvalbumin–restrictin colocalization, respectively) (Table 8).

The discrepancy between the results of PCC and MOC coefficients emphasized that conclusions about colocalization should not be made after calculating only a single coefficient and that if more coefficients are calculated, the more precise interpretation of the findings can be made. In this case, the authors concluded that even though PCC showed numbers indicating the absence of colocalization, all other coefficients, including the more applicable MOC, detected its presence and thus both pairs of parvalbumin–spectrin and parvalbumin–restrictin antigens should be considered colocalized.

In addition, quantitative analysis allowed to make a very interesting and not-otherwise-obtainable observation when applied to analysis of colocalization in individual neurons (Fig. 8). As mentioned above, selecting smaller areas on images, like in this case of selecting areas containing individual neurons, it is usually possible to obtain very accurate calculations, because smaller number of analyzed pixels in selected ROIs ensures that there is no data overflow during quantification sessions. Calculations of PCC and MOC coefficients revealed heterogeneity of neurons stained for pairs of parvalbumin–spectrin and parvalbumin–restrictin antigens.

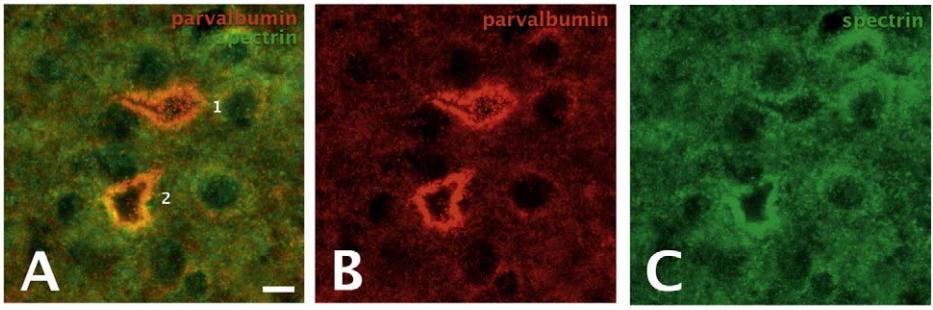

Fig. 8. Two neighbouring neurons showing different colocalization (A) of parvalbumin (B) and spectrin (C) in perineuronal nets. According to PCCs and MOCs, they were classified as the neurons with low (1) and moderate (2) degree of colocalization (details presented in Table 9). The scale bar indicates 20 μm (equally applicable to both images).

Based on coefficients results, it was possible to distinguish three different populations of neurons with high, moderate, and low degree of colocalization (Table 9).

This finding may indicate that the examined neurons are either distinctively different themselves or were analyzed in a different metabolic state. The latter can be due to the very dynamic nature of surrounding these neurons perineuronal nets. Biologically, this is an important finding to demonstrate that the values of colocalization in the same structures and under the same conditions are not always constant. It should be taken into consideration carefully when modeling/analyzing various (especially pathological) processes.

3.2. Quantification of colocalization between exogenous TLS and Nd1-L mRNA reveals that TLS-GFP is unable to rescue mRNP formation near spines and spine phenotype in TLS-KO

Quantitative colocalization analysis helped to reveal that formation of translocated in liposarcoma (TLS)-Nd1 mRNA complex clusters is impaired in TLS-deficient hippocampal neurons (Fujii et al., 2009). To reach this conclusion, the authors performed quantitative colocalization analysis of TLS-GFP and Nd1-L mRNA.

TLS is RNA-binding protein observed in the dendritic spines of mature hippocampal neurons (Belly et al., 2005; Fujii et al., 2005). It is associated with Nd1-L mRNA that encodes an actin-stabilizing protein (Sasagawa et al., 2002). It was found that although Nd1-L mRNA is expressed in TLS knock out mouse (TLS-KO) neurons, the amount of Nd1-L mRNA in the dendrites of TLS-KO neurons is significantly reduced (Fujii and Takumi, 2005). It was also previously shown that hippocampal neurons of TLS-KO exhibit abnormal spine morphology, which can be explained by an improper supply of specific dendritic mRNAs due to TLS deficiency (Fujii et al., 2005).

Table 9. Quantitative colocalization analysis helps to distinguish three distinctive populations of neurons with high, moderate, and low degree of colocalization.

Colocalized molecules	High degree (%)	Moderate degree (%)	Low degree (%)
Parvalbumin + spectrin	24.4 ± 1.2	46.3 ± 3	29.3 ± 2.5
Parvalbumin + restrictin	27 ± 1.6	55.1 ± 4.3	17.9 ± 0.8

Conclusions are based on calculations of PCC and MOC. The values of PCC above 0.5 and in the ranges from 0.2 to 0.5 and from 0 to 0.2, and the values of MOC in the ranges from 0.8 to 0.9, from 0.7 to 0.8, and from 0.6 to 0. 7 were assigned to high, moderate, and low degrees, respectively. Percentages of cells in each range in relation to all examined cells are shown. Fifty neurons were examined for each coefficient. Statistical comparisons were performed using the Mann–Whitney U test. $P < 0.05$.

By using CoLocalizer Pro software and calculating PCC, MOC, and k_1–k_2 coefficients on images of neurons, a significant decrease of colocalization in both dendrites and the spines of TLS-KO neurons was shown (Fujii et al., 2009). Moreover, the exogenous expression of TLS in TLS-KO neurons at the later stage did not compensate for the aberrant spine development. The authors concluded that a timely TLS expression is required for proper expression of Nd1-L in the neuronal dendrites and spine maturation.

Interestingly, quantification of colocalization in different portions of dendrites elegantly provided a unique piece of valuable information that in both wild and KO mice colocalization of TLS-GFP and Nd1-L mRNA is significantly higher in the distal parts of individual dendrites compared to their proximal parts (Fig. 9).

It should be mentioned that quantification of colocalization in this study was performed on fluorescence signals generated not by purely fluorochrome-conjugated antibodies, but a combination of alkaline phosphatase (AP) and fluorescence in situ hybridization (FISH). However, the results of calculations were within the range of standard values and proved to be reliable, thus showing good applicability of the quantification method in such cases as well.

3.3. Colocalization analysis helps to clarify the essential role of caveolin-1 for NMDAR localization to neuronal membrane rafts, NMDAR/Src tyrosine kinase family/ERK signaling, and protection of neurons from ischemic injury and cell death

Observation of colocalization and especially its quantification were crucial in understanding the role of caveolin-1 for N-methyl-D-aspartate receptor (NMDAR) localization and its involvement in protection of neurons from the impact of ischemia (Head et al., 2008).

Caveolin is known as a protein that scaffolds and regulates the multiple types of signaling molecules involved in coordinated, precise, and rapid regulation of cell functions (Lisanti et al., 1994; Couet et al., 1997; Ostrom et al., 2002). NMDAR is a subtype of excitatory glutamate receptors that play key roles in neuronal

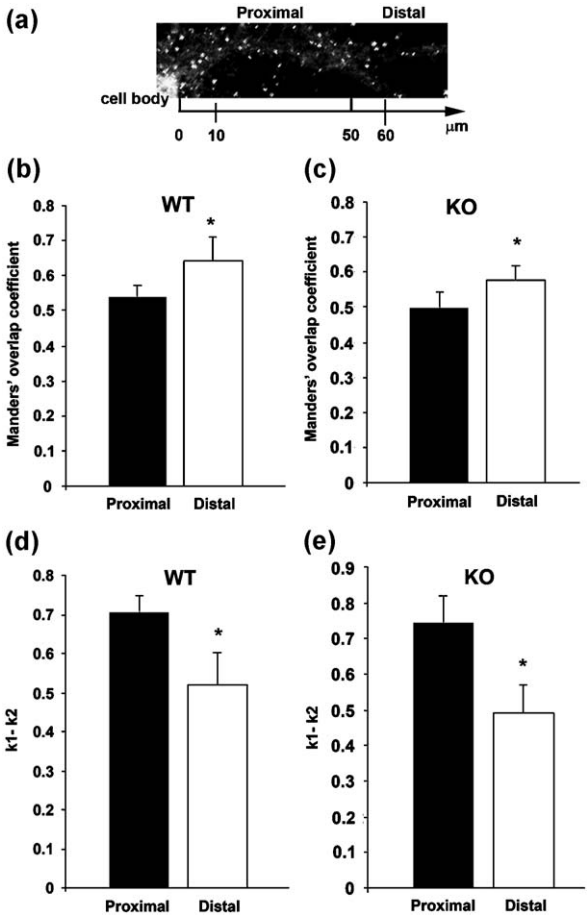

Fig. 9. Comparison of colocalization of TLS-GFP and Nd1-L mRNA in the proximal and distal parts of the neuronal dendrites (a) in the individual dendrites of wild-type (WT) and TLS-knock out (KO) mice. MOC (b and c, respectively) and pairs of k_1–k_2 overlap coefficients (d and e, respectively) were employed. Note significantly higher colocalization numbers in the distal parts of neurons for both WT and KO mice. $P<0.05$ (four dendrites from two independent experiments). Error bars indicate SEM. Reproduced from Fujii et al. (2009) with permission from Lippincott Williams & Wilkins.

development, plasticity, and excitotoxicity (Choi, 1988; McDonald and Johnston, 1990; Collingridge and Bliss, 1995). NMDAR activation was implicated in triggering cerebral preconditioning, a phenomenon by which stimuli, like sublethal ischemia or drugs, can protect the brain from subsequent lethal ischemia (Murry et al., 1986; Grabb and Choi, 1999; Rubino and Yellon, 2000; Soriano et al., 2006). It was also reported that caveolin serves as a substrate and scaffold for Src tyrosine kinases family (SFK)s, key regulators of NMDAR activity (Salter and Kalia, 2004).

However, the mechanisms controlling NMDAR-induced preconditioning were not understood.

The authors examined the pattern of colocalization of NMDAR type 2B (NMDAR2B) with caveolin-1 and cholera toxin B (CT-B), a membrane raft marker. After correcting background in CoLocalizer Pro software, MOCs were calculated and used for estimation of colocalization. A high degree of colocalization of NMDAR2B with caveolin-1 was found on both the cell body and along neuronal extensions resembling dendritic shafts and spines, both of which are highly enriched in NMDAR2B-containing NMDARs (Tovar and Westbrook, 1999). Because majority of NMDAR subtypes localize to neuronal membrane rafts (Besshoh et al., 2005), the authors performed immunofluorescence microscopy and subsequent quantification of colocalization to assess the presence of NMDAR2B in neuronal membrane rafts. It was observed that the vast majority (approximately 90%) of CT-B was colocalized with caveolin-1, while a half of caveolin-1 was colocalized with CT-B. At the same time, approximately 40% of CT-B and NMDARB were colocalized with each other. Further assessments using sucrose density fractionation showed that under basal conditions NMDAR2B is distributed to both buoyant, low-density fractions (BFs) and heavy fractions (HFs). After NMDA agonist stimulation NMDAR2B was redistributed to only HFs. Thus, in combination with sucrose density fractionation technique, quantitative colocalization analysis helped to establish the presence of NMDAR2Bs to neuronal membrane rafts and revealed their alterations by an agonist.

3.4. Increased colocalization of vesicular glutamate transporters 1 and 2 at single axon terminals

The question about biological significance of the presence of vesicular glutamate transporters 1 (VGLUT1) and 2 (VGLUT2) at single axon terminals during postnatal development of neocortex was addressed in the study that employed extensive quantitative colocalization assessments of the expression of VGLUT1 and VGLUT2 molecules in the brain of mice during development (Nakamura et al., 2007).

L-Glutamate is the major excitatory neurotransmitter that plays an important role in neocortical functions and is known for its involvement in the maturation of neocortical circuitry. Vesicular glutamate transporters catalyze the uptake of glutamate from cytoplasm to synaptic vesicles and are essential for glutamatergic transmission (Fremeau et al., 2001; Takamori, 2006). Among three mammalian isoforms of VGLUT, VGLUT1 is produced predominantly by neurons in telencephalic structures, while VGLUT2 is expressed mainly by neurons in diencephalic and lower regions of brain stem (Ni et al., 1995; Herzog et al., 2001; Hisano et al., 2000). Therefore, glutamatergic axon terminals of cortical and thalamic origins were suggested to preferentially display immunoreactivities of VGLUT1 and VGLUT2 in the neocortex (Fujiyama et al., 2001).

Based on their previous observations about transiently augmented colocalization of VGLUT1 and VGLUT2 in the primary somatosensory cortex during early

postnatal development (Nakamura et al., 2005), Nakamura et al. (2007) examined colocalization of VGLUT1 and VGLUT2 at single axon terminals with the purpose of determining the changes of its degree during postnatal development of the mouse neocortex (Fig. 10). The degree of colocalization was determined using PCC. The areas with colocalization were more frequently observed in the primary somatosensory (S1) area than in both the primary visual (V1) and the primary motor (M1) areas. When S1 cortical layers were examined, colocalization was most evident in the layer IV barrels at postnatal day (P) 7 and in the adulthood. In the layer IV, highest values of PCC were detected in area S1 at P7 and in the area V1 at P10 (data not shown). These observations revealed that thalamocortical axon terminals contain both VGLUT1 and VGLUT2, especially at P7-10. Importantly, these conclusions were confirmed by using the double FISH technique and detecting coexpression of VGLUT1 and VGLUT2 mRNA in the somatosensory thalamic nuclei at P7. Since VGLUT1 is frequently detected in axon terminals that show synaptic plasticity in the adult brain, the authors' findings suggested that VGLUT1 is used in thalamocortical axons transiently during the postnatal period when there is a need for plasticity.

In addition, Nakamura et al. (2007) also tested the impact of deconvolution on the results of coefficients calculations and found that deconvolution had little, if any, effect on the values of PCC (Fig. 11a–c).

3.5. Heterogenous distribution of synaptosomal-associated protein of 25 kDa revealed by quantitative analysis

The results of PCC and MOC coefficients were of considerable help in an insightful study of Garbelli et al. (2008) with focus on the pattern of expression of

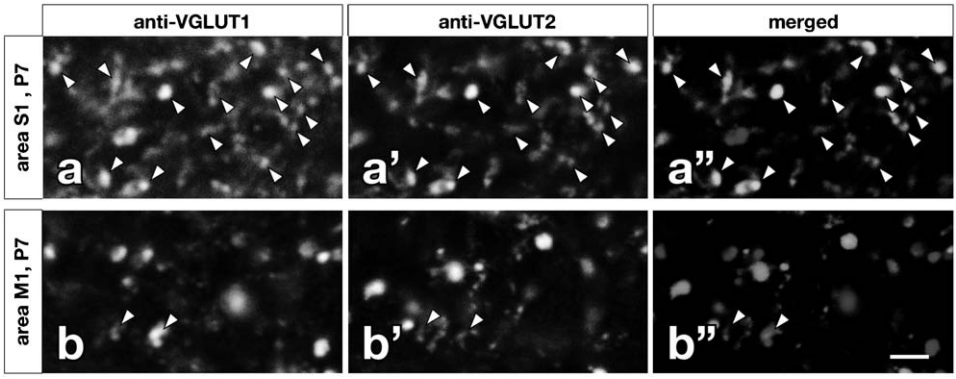

Fig. 10. Confocal micrographs showing colocalization of VGLUT1 and VGLUT2 in postnatal developing mouse brain. Alexa 647- and Alexa 488-labeled secondary antibodies were used for visualizing VGLUT1 (a, b) and VGLUT2 (a′, b′), respectively. Shots were taken at the layer IV barrels of areas S1 at P7 (a-a″) and M1 at P7 (b-b″). Merged images appear at a″ and b″, respectively. Arrowheads indicate the areas of colocalization at putative axon terminals. The scale bar indicates 2 μm (equally applicable to all images). Reproduced from Nakamura et al. (2007) with permission from Blackwell Publishing Ltd.

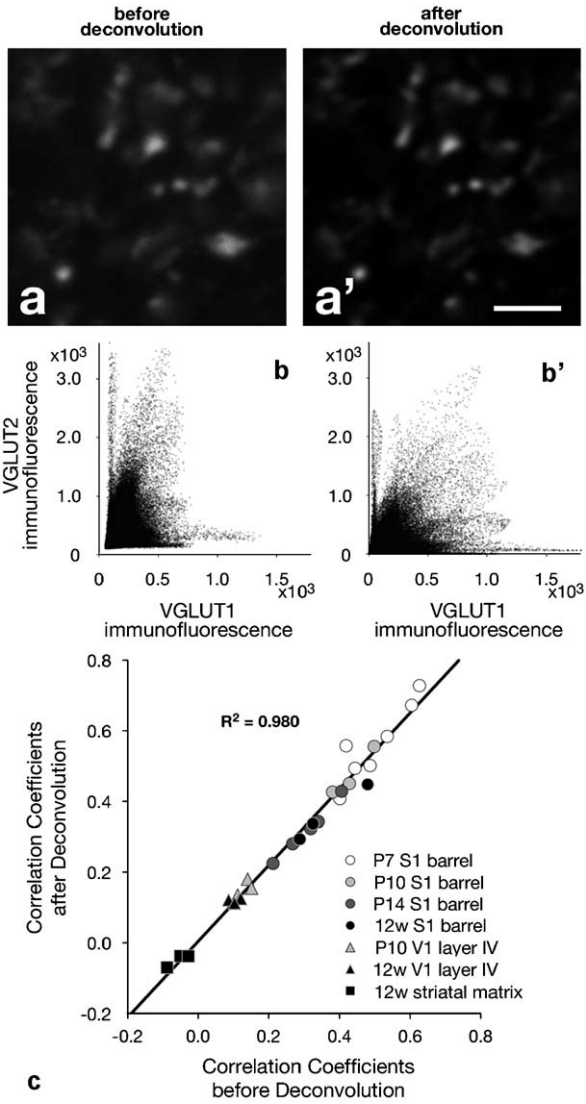

Fig. 11. Comparison of the appearance of analyzed images (a and a′), their respective scatter grams (b and b′), and the results of PCC calculations (c) before and after deconvolution procedure. Note little differences in either image and scatter grams appearance or PCC calculations results. Reproduced from Nakamura et al. (2007) with permission from Blackwell Publishing Ltd.

synaptosomal-associated protein of 25 KDa (SNAP-25) in the rat and human brain. SNAP-25 is a plasma membrane protein that together with syntaxin and the synaptic vesicle-associated membrane protein (VAMP)/synaptobrevin form the initial

SNARE (SNAP and NSF (N-ethylmaleimide sensitive fusion protein) attachment receptors) docking complex involved in the regulation of exocytosis (Jahn et al., 2003; Sudhof, 2004). During development, the expression of SNAP-25 correlates with synaptogenesis and neuronal maturation (Catsicas et al., 1991). Prior to synapse formation, SNAP-25 can be detected in cell bodies and fibers of the neonatal brain (Oyler et al., 1991). In the adult rat brain, however, SNAP-25 becomes undetectable due to protein segregation to presynaptic terminals (Geddes et al., 1990; Oyler et al., 1992) . Predominant localization of SNAP-25 at nerve terminals was confirmed by immunoelectron microscopy (Oyler et al., 1989; Duc and Catsicas, 1995).

Using a combined methodological approach consisting of multiple-labeling immunofluorescence, confocal microscopy, and immunoelectron histochemistry, Garbelli et al. (2008) examined the expression of SNAP-25 in excitatory and inhibitory terminals from different areas of rat and human brain. Glutamatergic and GABAergic terminals were identified by staining for the VGLUT1, glutamic acid decarboxylase of 67 kDa (GAD67) or the vesicular GABA transporter (VGAT). In all examined brain areas GABAergic terminals did not display detectable levels of SNAP-25, whereas glutamatergic terminals revealed a variable degree of immunostaining. Quantification of colocalization revealed a high degree of colocalization between SNAP-25 and VGLUT1. In contrast, a low degree of colocalization comparable to that of two completely unrelated antigens was obtained when quantifying colocalization of SNAP-25 and VGAT (Fig. 12). This interesting observation corroborates the findings of Grossenbacher-Zinchuk et al. (2008) about variable degree of colocalization of the components of extracellular matrix in the perineuronal nets of cortical parvalbumin-expressing neurons described above and may have important biological implications.

Importantly, the quantitative observations of Garbelli et al. (2008) were firmly supported by the results of ultrastructural immunohistochemical studies showing that a subset of glutamatergic synapses do not contain detectable levels of SNAP-25. This study provided the evidence that SNAP-25 expression is highly variable between different axon terminals both in rat and human brain and helped to conclude that heterogenous distribution of SNAP-25 may have important implications not only in relation to the function of the protein as SNARE, but also in the control of network excitability (Garbelli et al., 2008).

3.6. Distribution of glutamate receptor subunits 1–3 analyzed by quantitative colocalization helps to define the cellular basis for plasticity underlying the development of behavioral sensitization

Quantitative colocalization analysis played a central role in another study that investigated the role of alpha-amino-3-hydroxy-5-methyl-4-isoxazolepropionic acid (AMPA) receptor (AMPAR) trafficking in dopamine (DA) neurons under control conditions and after elevation of DA levels mimicking cocaine exposure (Gao and Wolf, 2007).

DA neurons of the ventral tegmental area (VTA) project to the nucleus accumbens, prefrontal cortex (PFC), and other corticolimbic regions and mediate responses to rewards and reward-predicting stimuli (Schultz, 2007). Glutamate receptors, arising from different brain regions, provide an important source of excitatory drive to these neurons (Carr and Sesack, 2000; Geisler et al., 2007). Excitatory synapses onto DA neurons of VTA represent a critical site of psychostimulant-induced synaptic plasticity. This plasticity involves alterations in synaptic strength through AMPAR redistribution.

With the help of a specially developed in vitro model, Gao and Wolf (2007) studied regulation of AMPAR trafficking in DA neurons under control conditions and after elevation of DA levels that mimic the exposure to cocaine. The model used cocultures containing rat VTA and PFC neurons obtained from enhanced cyan

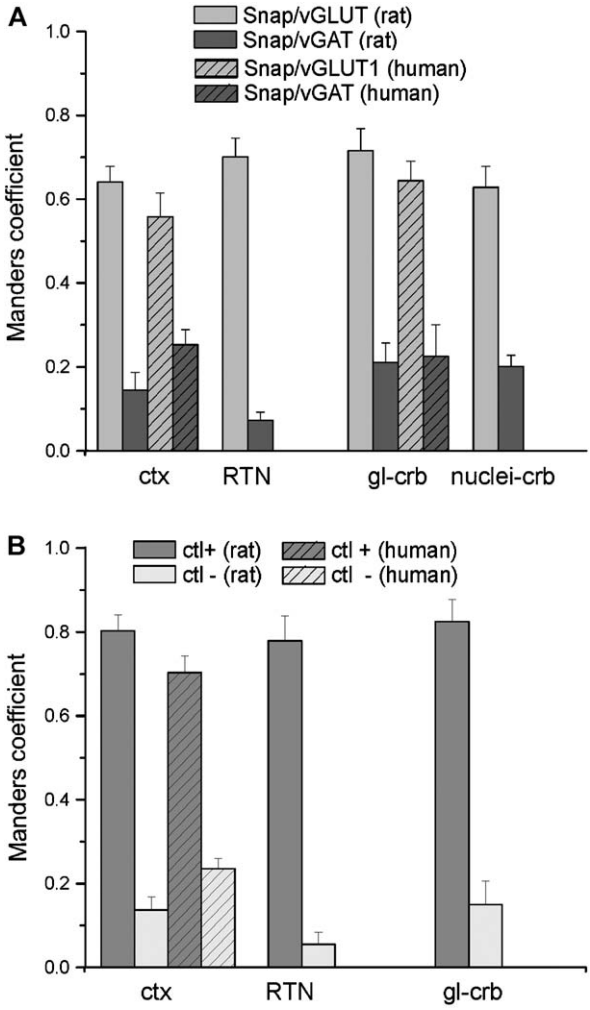

fluorescent protein-expressing mice. It was found that in VTA-PFC cocultures, D_1 receptor activation for 10 min increased synaptic and nonsynaptic glutamate receptor subunit 1 (GLUR1) and GLUR2 surface expression on DA neurons. N-methyl-D-aspartic acid (NMDA) or AMPA receptor antagonists blocked this effect, and it was not observed in pure VTA cultures, suggesting that DA agonists acted on D_1 receptors on PFC neurons, altering their excitatory transmission onto VTA DA neurons and, therefore, influencing AMPARs. To mimic the longer elevation in extracellular DA levels produced by systemic exposure to cocaine, cocultures were incubated with DA for 1 h. Synaptic GLUR1 was increased 24 h later, reminiscent of the increased AMPA/NMDA ratio at excitatory synapses onto VTA DA neurons 24 h after cocaine injection (Ungless et al., 2001). In contrast, GLUR2 remained unchanged. Gao and Wolf (2007) then elegantly applied quantitative colocalization analysis to examine the surface expression of GLUR1-3 (Fig. 13). They showed that DA neurons express a substantial number of GLUR1/2, GLUR2/3, and homomeric GLUR1 receptors and that the increase in surface AMPARs 24 h after DA exposure may reflect increased GLUR1/3-containing receptors. Thus, these results helped to define the cellular basis for plasticity underlying the development of behavioral sensitization (Gao and Wolf, 2007).

3.7. Uncovering a unique colocalization relationship between substance P and GABA in the central nucleus of amygdala

Quantification of colocalization helped to obtain a decisive piece of evidence showing a special colocalization relationship between substance P and GABA in the central amygdalar nucleus (Shigematsu et al., 2008).

Fig. 12. Values of MOC characterizing the degree of colocalization between SNAP-25/vGLUT1 (light gray bars), SNAP-25/vGAT (dark gray bars), SNAP-25/vGLUT1 (striped light gray bars), and SNAP-25/vGAT (striped dark gray bars) in the rat and human samples, respectively (A). As a comparison, the values of the coefficient characterizing the degree of colocalization between a vesicle-associated membrane protein 2 and synaptotagmin I (VAMP-2 and Syt I) (positive control, dark gray bars) and neurofilament marker SMI311 and connexin 43 (negative control, light gray bars) in the rat and human (striped bars) samples are given (B). Note the high degree of colocalization between SNAP-25/vGLUT1 (presented in percentage points as 55–71% and VAMP-2/Syt I (70–82%). At the same time, the degree of overlap between SNAP-25 and vGAT (7–25%) is not significantly different than that of unrelated antigens, such as connexin 43, which is localized on glial processes, and SMI311, which is localized in neuronal cells (5–23%). This observation suggests the possibility that, in addition to high, a low degree of colocalization of SNAP and vGAT can occasionally occur as well. An average $\pm$ SD of coefficients of each analyzed area is given. Abbreviations are as follows: cerebral cortex (ctx), glomerular layer of cerebellum (gl-crb), deep cerebellar nuclei (nuclei-crb), reticular thalamic nucleus (RTN). Reproduced from Garbelli et al. (2008) with permission from Wiley-Liss, Inc.

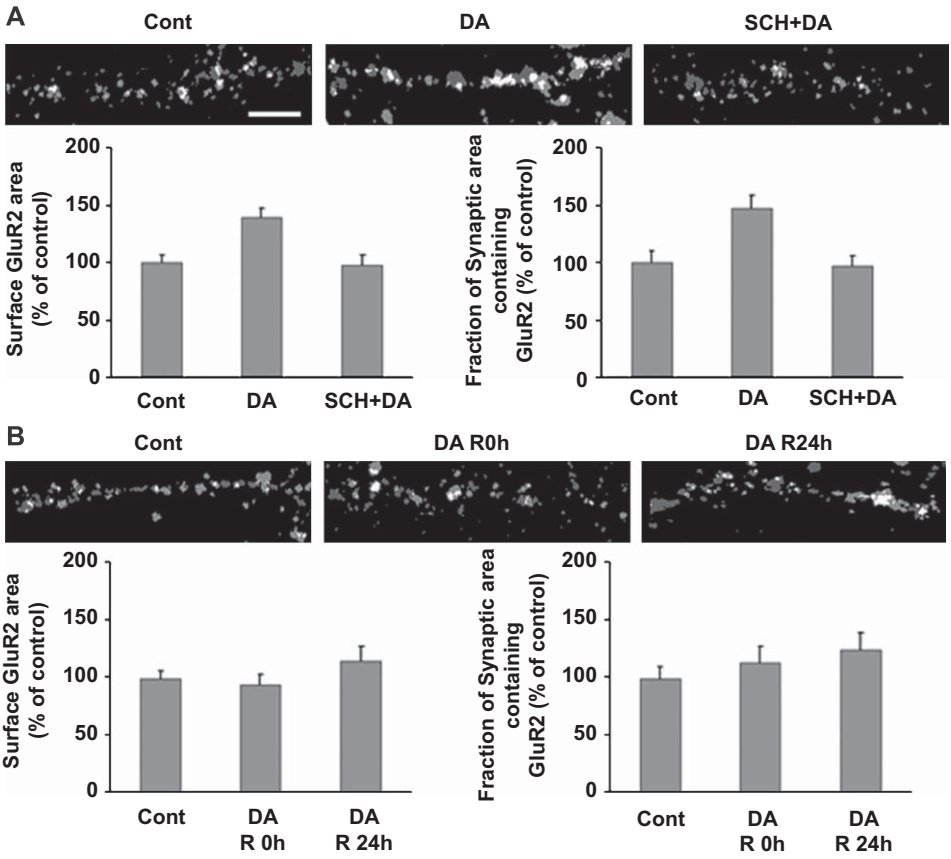

Fig. 13. Increase of GLUR2 surface and synaptic expression by DA neurons after brief (10 min), but not prolonged (1 h) incubation with DA. (A) VTA-PFC cocultures were treated with media (Cont), in the presence of DA (DA), and after R-(+)-7-chloro-8-hydroxy-3-methyl-1-phenyl-2,3,4,5-tetrahydro-1H-3-benzazepine hydrochloride (SCH 23390) (SCH + DA) was added. Images indicate colocalization of GLUR2 and synaptophysin; graphs show quantification of surface GLUR2 staining and the portion of synaptic area containing GLUR2. Increase of surface and synaptic expression by DA is blocked by SCH 23390. $P < 0.05$. (B) VTA-PFC cocultures were treated with media (Cont) and DA for 0 h (DA R 0 h) and 24 h (DA R 24 h). Images indicate colocalization of GLUR2 and synaptophysin; graphs show quantification of surface GLUR2 staining and the portion of synaptic area containing GLUR2. In contrast to the results for GLUR1 (data not shown), surface and synaptic expression of GLUR2 were not altered by the prolonged treatment. $P > 0.05$. The scale bar indicates 5 μm (equally applicable to all images). Reproduced from Gao and Wolf (2007) with permission from the Society of Neuroscience.

Substance P (SP) is a neuropeptide found in axon terminals (Nawa et al., 1983; Kawaguchi et al., 1986). Although it is known that various neurotransmitters coexist together with SP in the mammalian brains, there was no knowledge about the

relationship between them in the central nucleus of amygdala (CeA), where both SP and its receptors are concentrated to a high degree. CeA works as an output device of amygdala and sends information processed in the amygdala to hypothalamus and brain stem nuclei, thereby mediates the expression of emotions (Davis, 1998; LeDoux, 2000). Importantly, CeA is also related to pathological conditions, such as depression. It was reported that selective antagonists to neurokinin1 (NK1), an SP-specific receptor, display antidepressant effects (Kramer et al., 1998). Although both SP (Nilsson et al., 1974; Emson et al., 1978) and NK1 receptors (Mantyh et al., 1989; Nakaya et al., 1994) are abundant in CeA, it remained unknown whether (and if yes which of them and to what degree) any classical neurotransmitters are expressed in SP-containing terminals.

To address this question, Shigematsu et al. (2008) combined light and electron microscopical immunohistochemistry with quantitative colocalization analysis to examine the detailed pattern of expression of a range of neurotransmitters. Weak immunostaining for glutamic acid decarboxylase (GAD), the GABA synthetic enzyme, was found in the majority of SP-positive boutons in CeA. Definite staining was detected in SP-containing boutons in the reticular part of substantia nigra (data not shown). Electron microscopy demonstrated small clear vesicles in addition to dense core vesicles within SP-positive terminals that formed symmetrical synapses, indicating the presence of some classical transmitter, most likely GABA. Quantitative colocalization analysis was applied by analyzing immunoreactivity of VGLUT- and SP-positive boutons. Importantly, the results of immunofluorescence studies were confirmed by electron microscopical observations of SP immunoreactivity.

Taken together, the data obtained using this combined methodological approach helped to reveal a unique mode of synaptic transmission at amygdalar SP-containing terminals where slowly acting SP is concentrated, but both GABA and its synthetic enzyme are maintained at low levels. This pattern may underline the unique nature of long-lasting responses in emotions.

3.8. Elimination of synapses accompanies functional plasticity of hippocampal neurons

Applications of quantitative colocalization are particularly informative when studying dynamical regulatory processes in the nervous system. This was convincingly shown by investigating changes occurring in the synapses of hippocampal neurons (Bastrikova et al., 2008).

It is known that overproduction of synapses and their subsequent elimination through activity- and experience-dependent processes are crucial for refinement of neuronal circuits during development (Hua and Smith, 2004). As it was reported on the example of mammalian visual cortex, pruning of geniculocortical synapses occurs in response to monocular visual deprivation (MD) during critical postnatal periods (Hubel et al., 1977). Neuronal activity is important for this type of synapse elimination, because blockade of action potentials in the cortex completely prevents synaptic loss and restructuring after MD (Reiter et al., 1986; Stryker and Harris,

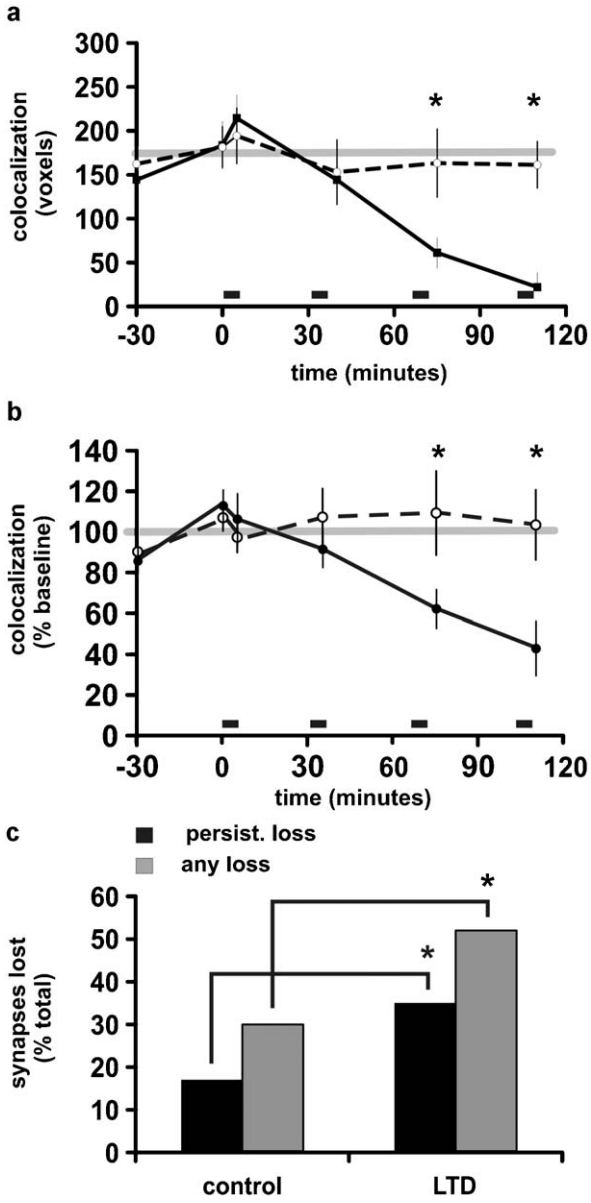

Fig. 14. Decrease of colocalization of pre- and postsynaptic structures and increase in separation of synapses after LTD. (a) Average red/green (presynaptic/postsynaptic) colocalization over time is shown for both unstimulated control cases and synapses in which LTD exceeded 15%. One pixel volume (voxel) is equal to $0.0007\,\mu m^3$. Low-frequency stimulation is indicated by the bars. (b) Data expressed as a percentage of baseline values are shown. $P<0.01$, $^*P<0.05$. (c) LTD-inducing stimulation enhanced both persistent and temporary loss of putative synapses. Reproduced from Bastrikova et al. (2008). Originally appeared in the Proceedings of the National Academy of Sciences of the United States of America, protected by the respective copyright.

1986) Furthermore, the loss of synapses requires NMDA receptors, suggesting that postsynaptic processes are important as well (Gu et al., 1989; Bear et al., 1990; Colonnese and Constantine-Paton, 2006). These findings therefore show that elimination of synapses is an active process, not just a consequence of nonuse (Lichtman and Colman, 2000).

Changes in synaptic strength in the form of long-term potentiation (LTP) and long-term depression (LTD) correlate with dendritic spine enlargement or shrinkage, but it remains unknown whether LTD can lead to an actual separation of the synaptic structures when the spine shrinks or is lost. Bastrikova et al. (2008) addressed this issue by using concurrent imaging and electrophysiological recording of live synapses. Methodologically, slices of rat hippocampus were cultured on multielectrode arrays, and the neurons were labeled with genes encoding red and green fluorescent proteins to visualize pre- and postsynaptic neuronal processes, respectively. LTD-inducing stimulation led to a decrease of synaptic red/green colocalization and in many cases also induced a complete separation of the presynaptic bouton from the dendritic spine. This type of synapse loss was associated with smaller initial spine size and greater synaptic depression, but not spine shrinkage during LTD. In all cases, separation of synapses was observed without an accompanying loss of the spine. Colocalization was calculated between spines and axonal boutons by manually constructing the outline of ROI around each spines or synapses and then applying corresponding algorithms to these areas. Its degree was assessed using PCC.

It was revealed that LTD decreases colocalization of pre- and postsynaptic structures and increases separation of synapses (Fig. 14). This type of synapse loss was associated with smaller initial spine size and greater synaptic depression, but not with spine shrinkage. The authors concluded that repeated low-frequency stimulation simultaneous with LTD induction is capable of restructuring synaptic contacts. This conclusion led to important suggestion that the rapid activity-dependent refinement of neuronal circuitry during development is likely occurring throughout cerebral cortex. The finding that small initial dendritic spine size predicts a higher likelihood of synapse loss could help explain why problems with spine maturation during development could lead to a profound impact on the circuitry of adult brain (Bastrikova et al., 2008).

3.9. Quantitative analysis provides new insights into molecular composition of distinct spinal muscular atrophy multiprotein complexes in neurons

Basic medico-biological research is not the only field benefiting from the applications of quantitative colocalization analysis. As Zhang et al. (2006) convincingly showed on the example of spinal muscular atrophy (SMA), quantification is highly applicable to clinically oriented studies as well.

SMA is a common inherited disease characterized by neurodegeneration of α-motor neurons (Frugier et al., 2002). It is caused by mutation and/or deletion of the *SMN1* gene encoding the survival of motor neuron protein (SMN) (Frugier et al., 2002). SMN localizes to both the cytoplasm and the nucleus. In the nucleus, it is

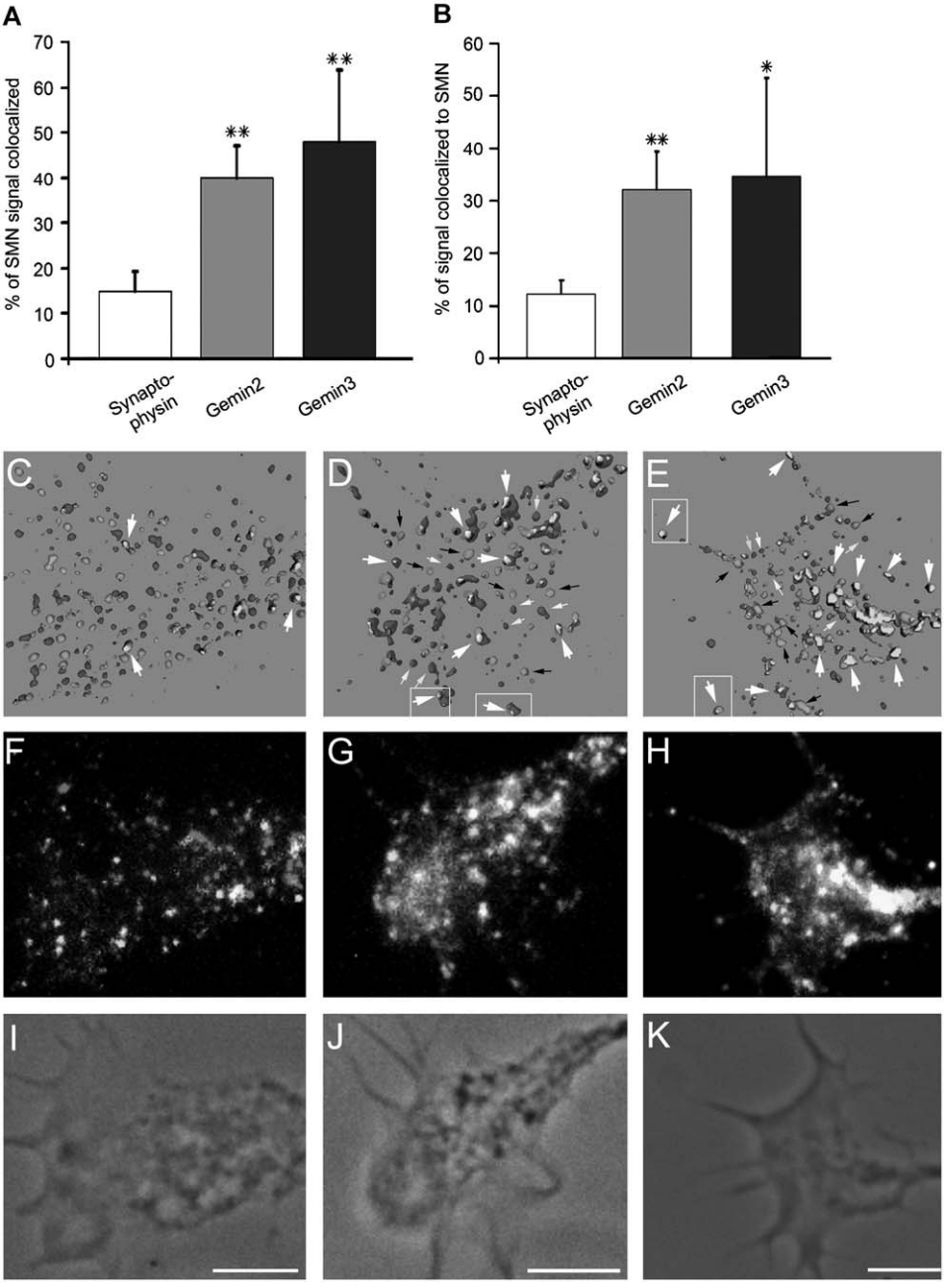
A
% of SMN signal colocalized
70
60
50
40
30
20
10
0
**
**
Synapto-physin
Gemin2
Gemin3
B
% of signal colocalized to SMN
60
50
40
30
20
10
0
**
*
Synapto-physin
Gemin2
Gemin3
C
D
E
F
G
H
I
J
K

detected in gems (Liu, Dreyfuss, 1996) that frequently colocalize with coiled (Cajal) bodies (Carvalho et al., 1999; Young et al., 2000). Biochemical studies using non-neuronal cell lines, identified several SMN-associated proteins, named Gemins (Gubitz et al., 2004). These proteins were shown to be integral components of the SMN ribonucleoprotein complex (Yong et al., 2004). It was also hypothesized that an additional function of SMN in neurons can be to facilitate assembly of small nuclear ribonucleoprotein (RNP)s (snRNPs).

For understanding of the mechanism of SMN involvement in the assembly and/or localization of RNP complexes in neurons, it is first necessary to identify the protein composition of SMN granules and explore their interactions with SMN at the molecular level. Previous studies did not obtain any conclusive information on whether Gemin proteins are present in the form of particles within neuronal processes and whether they colocalize with SMN. One study reported a specific pattern of distribution of SMN in processes of cultured motor neurons, while Sip1 (Gemin2) revealed a uniform distribution and little colocalization (Jablonka et al., 2001). Another more recent study used immunofluorescence microscopy and detected the presence of SMN and several Gemin proteins coenriched in neuritic protrusions of PC12 cells (cancer cells derived from a pheochromocytoma of the rat adrenal medulla and used as a model for neuronal differentiation) (Sharma et al., 2005). However, no attempt was made to elucidate whether SMN and Gemins coexist within individual particles and granules. Therefore, Zhang et al. (2006) employed immunofluorescence microscopy combined with quantitative colocalization analysis and FRET of live and fixed neurons to examine SMN–Gemin complexes in neuritic granules.

It was found that SMN is localized in granules that are actively transported into neuronal processes and growth cones. Interestingly, in cultured motor neurons, SMN granules showed colocalization with RNP Gemin proteins, but not with spliceosomal Sm proteins needed for snRNP assembly (Zhang et al., 2006). Quantification of colocalization was performed after 3D reconstruction of images and showed approximately 40% colocalization of SMN with Gemin2 and 50% colocalization

Fig. 15. Quantification of SMN-Gemin colocalization in growth cones following 3D reconstruction. Hippocampal neurons were cultured and processed for immunostaining using corresponding antibodies. Growth cones were imaged in 3D. After deconvolution and background correction, images were processed for quantitative colocalization analysis. (A) Colocalization of SMN with synaptophysin, Gemin2, and Gemin3 constituted $15 \pm 4.5\%$, $40.0 \pm 7.0\%$, and $47.8 \pm 15.8\%$, respectively. (B) The Gemin2 signal ($32.3 \pm 7.2\%$) was 1.6 times higher than the synaptohysin signal ($12.3 \pm 2.6\%$) colocalized to SMN, and Gemin3 signal ($34.7 \pm 18.8\%$) colocalized to SMN was 1.8 times higher than synaptophysin signal ($12.3 \pm 2.6\%$). $^{*}P < 0.01$, $^{**}P < 0.001$. The patterns of colocalization of SMN with synaptophysin, Gemin2, and Gemin3 are represented by deconvoluted and reconstructed images shown in C, D, and E, respectively. Colocalized areas are indicated by white arrows (Gemin2 and Gemin3). F–H show the respective raw images. I–K represent corresponding phase contrast images. Scale bars indicate 5 μm. Reproduced from Zhang et al. (2006) with permission from the Society of Neuroscience.

with Gemin3 (Fig. 15). SMN- and Gemin-containing granules were seen distributed to both dendrites and axons of differentiated motor neurons. The use of FRET technique revealed direct interaction between SNM and Gemin2 within single granules. In addition, high-speed dual channel imaging of live neurons indicated the rapid and bidirectional transport of the SMN–Gemin complex. The N terminus of SMN was needed for the recruitment of Gemin2 into cytoplasmic granules and enhanced Gemin2 stability. Taken together, these findings provided new insights into molecular composition of distinct SMN multiprotein complexes in neurons and laid ground for further studies to investigate a clinical significance of localized RNPs in SMN.

3.10. Fluorescent protein expression and colocalization on single secretory vesicles in mouse cortical astrocytes can be detectable using linear spectral unmixing

The efforts to properly quantify colocalization frequently coincide with the need to improve and further develop the analytical tools required. This was the case in the recent study that addressed the issue of incomplete separation of the different colour channels due to the presence of autofluorescence (Nadrigny et al., 2006).

Nadrigny et al. (2006) introduced a new live cell epifluorescence spectral imaging and linear unmixing technique to classify resolution-limited point objects containing multiple fluorophores. Spectral unmixing is a technique that quantifies the presence of several fluorophores in mixed pixels. It assigns a mixed pixel the fluorescence which the pixel would have had if it consisted of a pure spectral component only (Bosdogianni and Petrou, 1997). The advantages of this technique were demonstrated by showing the high overlap of coexpression of the vesicle-associated membrane protein 2 (VAMP2), also known as synaptobrevin2, linked to either enhanced green fluorescent protein (EGFP) or citrine (a less pH-sensitive variant of enhanced yellow fluorescent protein (EYFP), in mouse cortical astrocytes. In contrast, the coexpression of VAMP2-citrine and fused to EGFP lysosomal transporter sialine, showed little overlap. The use of spectral imaging and linear unmixing allowed fingerprinting the expression of spectrally overlapping proteins on single secretory organelles in the presence of spectrally broad autofluorescence. Thus, this approach provided a viable alternative to conventional colocalization studies.

4. Summary and conclusions

Quantitative analysis of colocalization has established its place as an important tool in the arsenal of modern cell and molecular biological analytical techniques. In this review, we presented information about colocalization condensed towards its practically oriented fundamentals. The following should be remembered when performing quantitative colocalization studies:

(1) although measurements of colocalization are accompanied by certain limitations, colocalization studies are capable of providing unique information not otherwise obtainable using other techniques,

(2) for maximum applicability, colocalization analysis should be used in combination with other morphological, physiological, immunological, etc. tools,
(3) to be precise and substantiated, conclusions about the degree of colocalization should not be limited to one coefficient, but should be based on the results of calculation of several (as many as) possible coefficients characterizing it.

In the provided examples, we showed practical cases of how quantification of colocalization was executed in the field of neuroscience. It is our hope that lessons learnt in those described examples can serve as a hands-on guide for researchers working in this field.

5. Future perspectives – refining image acquisition, perfecting analyzing techniques, and systematizing collected data

Despite the remarkable accomplishments, both theoretical and practical, quantitative colocalization technique continues to remain a work in progress, requiring further developments. The most important of them should be improvements of the quality of images to be analyzed and introduction of new background correction and colocalization coefficients algorithms. Actually useful background correction algorithms should be applicable to still images and capable of correcting background by distinguishing properties in images of tissue sections versus images of cells in culture. Improved colocalization algorithm (s) should have enhanced sensitivity, ignore differences of fluorescence intensities between channels, and deal with the bleed-through effect.

Even more importantly, quantitative colocalization analysis requires a more systematic approach in interpretation of obtained results. Presented in this review table with interpretation of results of coefficients calculations in relation to either presence or absence of colocalization shows the first step we have taken towards creation of a unified data base of colocalization information of various molecules. As a second step, we have already started collecting information about colocalization patterns of various commonly studied molecules with respect to the studied biological processes and tissues, employed colocalization coefficients, and used hard- and software. Accumulation of this information should be able to streamline cell and molecular biological research by serving as a unique quantitative colocalization reference data base.

Useful websites

- Website of CoLocalization Research Software, creators of CoLocalizer Pro, popular quantitative colocalization analysis software application – http://homepage.mac.com/colocalizerpro/
- Current Protocols in Cell Biology, a highly relevant source of comprehensive protocols in the fields of immunofluorescence labeling, confocal microscopy,

and quantitative imaging – http://www.mrw.interscience.wiley.com/emrw/9780471143031/cp/cpcb/toc
- MacResearch, online community and resource for Mac OS X in science – http://www.macresearch.org/

Acknowledgements

We would like to thank authors whose articles were used as examples of quantification of colocalization for valuable assistance during preparation of the manuscript, especially to Drs.: Ritsuko Fujii (Waseda-Olympus Bioscience Research Institute, Singapore), Brian P. Head (Department of Anesthesiology, University of California, San Diego, La Jolla, California, USA), Kouichi Nakamura (Department of Morphological Brain Science, Kyoto University, Kyoto, Japan), Carolina Frassoni (Clinical Epileptology and Experimental Neurophysiology Unit, Istituto Neurologico "C. Besta", Milan, Italy), Marina E. Wolf (Department of Neuroscience, The Chicago Medical School at Rosalind Franklin University of Medicine and Science, Chicago, USA), Takaichi Fukuda (Department of Anatomy and Neurobiology, Kyushu University, Fukuoka, Japan), Serena M. Dudek (Laboratory of Neurobiology, National Institute of Environmental Health Sciences, National Institute of Health, USA), Gary J. Bassell (Department of Cell Biology and Center for Neurodegenerative Disease, Emory University, Atlanta, USA), Martin Oheim (Molecular and Cellular Biophysics of Synaptic Transmission, Laboratory of Neurophysiology and New Microscopies, Université René Descartes, Paris, France). Observations describing varying colocalization of extracellular matrix components in the perineuronal nets of cortical parvalbumin-expressing neurons were partially presented in an invited lecture at 13th Congress of the International Federation of Societies for Histochemistry and Cytochemistry, Gdansk, Poland, 2008.

References

Adler J, Pagakis SN, Parmryd I. Replicate-based noise corrected correlation for accurate measurements of colocalization. J Microsc 2008;230:121–33.

Bastrikova N, Gardner GA, Reece JM, Jeromin A, Dudek SM. Synapse elimination accompanies functional plasticity in hippocampal neurons. Proc Natl Acad Sci U S A 2008;105:3123–7.

Bear MF, Kleinschmidt A, Gu QA, Singer W. Disruption of experience-dependent synaptic modifications in striate cortex by infusion of an NMDA receptor antagonist. J Neurosci 1990;10:909–25.

Belly A, Moreau-Gachelin F, Sadoul R, Goldberg Y. Delocalization of the multifunctional RNA splicing factor TLS/FUS in hippocampal neurones: exclusion from the nucleus and accumulation in dendritic granules and spine heads. Neurosci Lett 2005;379:152–7.

Besshoh S, Bawa D, Teves L, Wallace MC, Gurd JW. Increased phosphorylation and redistribution of NMDA receptors between synaptic lipid rafts and post-synaptic densities following transient global ischemia in the rat brain. J Neurochem 2005;93:186–94.

Bosdogianni P, Petrou M. Mixed pixel classification with robust statistics. IEEE Trans Geosci Remote Sens 1997;35:551–9.

Carr DB, Sesack SR. Projections from the rat prefrontal cortex to the ventral tegmental area: target specificity in the synaptic associations with mesoaccumbens and mesocortical neurons. J Neurosci 2000;20:3864–73.

Carvalho T, Almeida F, Calapez A, Lafarga M, Berciano MT, Carmo-Fonseca M. The spinal muscular atrophy disease gene product, SMN: A link between snRNP biogenesis and the Cajal (coiled) body. J Cell Biol 1999;147:715–28.

Catsicas S, Larhammar D, Blomqvist A, Sanna PP, Milner RJ, Wilson MC. Expression of a conserved cell-type-specific protein in nerve terminals coincides with synaptogenesis. Proc Natl Acad Sci U S A 1991;88:785–9.

Chen TW, Lin BJ, Brunner E, Schild D. In situ background estimation in quantitative fluorescence imaging. Biophys J 2006;90:2534–47.

Choi DW. Calcium-mediated neurotoxicity: relationship to specific channel types and role in ischemic damage. Trends Neurosci 1988;11:465–9.

Collingridge GL, Bliss TV. Memories of NMDA receptors and LTP. Trends Neurosci 1995;18:54–6.

Colonnese MT, Constantine-Paton M. Developmental period for N-methyl-D-aspartate (NMDA) receptor-dependent synapse elimination correlated with visuotopic map refinement. J Comp Neurol 2006;494:738–51.

Costes SV, Daelemans D, Cho EH, Dobbin Z, Pavlakis G, Lockett S. Automatic and quantitative measurement of protein–protein colocalization in live cells. Biophys J 2004;86:3993–4003.

Couet J, Sargiacomo M, Lisanti MP. Interaction of a receptor tyrosine kinase, EGF-R, with caveolins. Caveolin binding negatively regulates tyrosine and serine/threonine kinase activities. J Biol Chem 1997;272:30429–38.

Davis M. Anatomic and physiologic substrates of emotion in an animal model. J Clin Neurophysiol 1998;15:378–87.

Demandolx D, Barois N, Davoust J. Guidelines for multifluorescence confocal imaging: acquisition, processing and display. Eur Microsc Anal 1997;7:5–7.

Dityatev A, Bruckner G, Dityateva G, Grosche J, Kleene R, Schachner M. Activity-dependent formation and functions of chondroitin sulfate-rich extracellular matrix of perineuronal nets. Dev Neurobiol 2007;67:570–88.

Duc C, Catsicas S. Ultrastructural localization of SNAP-25 within the rat spinal cord and peripheral nervous system. J Comp Neurol 1995;356:152–63.

Emson PC, Jessell T, Paxinos G, Cuello AC. Substance P in the amygdaloid complex, bed nucleus and stria terminalis of the rat brain. Brain Res 1978;149:97–105.

Fremeau Jr RT, Troyer MD, Pahner I, Nygaard GO, Tran CH, Reimer RJ, et al. The expression of vesicular glutamate transporters defines two classes of excitatory synapse. Neuron 2001;31:247–60.

Fricker M, Runions J, Moore I. Quantitative fluorescence microscopy: from art to science. Annu Rev Plant Biol 2006;57:79–107.

Frugier T, Nicole S, Cifuentes-Diaz C, Melki J. The molecular bases of spinal muscular atrophy. Curr Opin Genet Dev 2002;12:294–8.

Fujii R, Grossenbacher-Zinchuk O, Jamari I, Wang Y, Zinchuk V, Takumi T. TLS-GFP cannot rescue mRNP formation near spines and spine phenotype in TLS-KO. Neuroreport 2009;20: 57–61.

Fujii R, Okabe S, Urushido T, Inoue K, Yoshimura A, Tachibana T, et al. The RNA binding protein TLS is translocated to dendritic spines by mGluR5 activation and regulates spine morphology. Curr Biol 2005;15:587–93.

Fujii R, Takumi T. TLS facilitates transport of mRNA encoding an actin-stabilizing protein to dendritic spines. J Cell Sci 2005;118:5755–65.

Fujiyama F, Furuta T, Kaneko T. Immunocytochemical localization of candidates for vesicular glutamate transporters in the rat cerebral cortex. J Comp Neurol 2001;435:379–87.

Gao C, Wolf ME. Dopamine alters AMPA receptor synaptic expression and subunit composition in dopamine neurons of the ventral tegmental area cultured with prefrontal cortex neurons. J Neurosci 2007;27:14275–85.

Garbelli R, Inverardi F, Medici V, Amadeo A, Verderio C, Matteoli M, et al. Heterogeneous expression of SNAP-25 in rat and human brain. J Comp Neurol 2008;506:373–86.

Geddes JW, Hess EJ, Hart RA, Kesslak JP, Cotman CW, Wilson MC. Lesions of hippocampal circuitry define synaptosomal-associated protein-25 (SNAP-25) as a novel presynaptic marker. Neuroscience 1990;38:515–25.

Geisler S, Derst C, Veh RW, Zahm DS. Glutamatergic afferents of the ventral tegmental area in the rat. J Neurosci 2007;27:5730–43.

Goucher DR, Wincovitch SM, Garfield SH, Carbone KM, Malik TH. A quantitative determination of multi-protein interactions by the analysis of confocal images using a pixel-by-pixel assessment algorithm. Bioinformatics 2005;21:3248–54.

Grabb MC, Choi DW. Ischemic tolerance in murine cortical cell culture: critical role for NMDA receptors. J Neurosci 1999;19:1657–62.
Grossenbacher-Zinchuk O, Celio M, Zinchuk V. Varying colocalization of extracellular matrix components in the perineuronal nets of cortical parvalbumin-expressing neurons revealed by quantitative analysis. Fol Histochem Cytobiol 2008;46:L068.
Gu QA, Bear MF, Singer W. Blockade of NMDA-receptors prevents ocularity changes in kitten visual cortex after reversed monocular deprivation. Brain Res Dev Brain Res 1989;47:281–8.
Gubitz AK, Feng W, Dreyfuss G. The SMN complex. Exp Cell Res 2004;296:51–6.
Halbhuber KJ, Konig K. Modern laser scanning microscopy in biology, biotechnology and medicine. Ann Anat 2003;185:1–20.
Head BP, Patel HH, Tsutsumi YM, Hu Y, Mejia T, Mora RC, et al. Caveolin-1 expression is essential for N-methyl-D-aspartate receptor-mediated Src and extracellular signal-regulated kinase 1/2 activation and protection of primary neurons from ischemic cell death. FASEB J 2008;22:828–40.
Herzog E, Bellenchi GC, Gras C, Bernard V, Ravassard P, Bedet C, et al. The existence of a second vesicular glutamate transporter specifies subpopulations of glutamatergic neurons. J Neurosci 2001;21:RC181.
Hisano S, Hoshi K, Ikeda Y, Maruyama D, Kanemoto M, Ichijo H, et al. Regional expression of a gene encoding a neuron-specific Na(+)-dependent inorganic phosphate cotransporter (DNPI) in the rat forebrain. Brain Res Mol Brain Res 2000;83:34–43.
Hua JY, Smith SJ. Neural activity and the dynamics of central nervous system development. Nat Neurosci 2004;7:327–32.
Hubel DH, Wiesel TN, LeVay S. Plasticity of ocular dominance columns in monkey striate cortex. Philos Trans R Soc Lond B Biol Sci 1977;278:377–409.
Jablonka S, Bandilla M, Wiese S, Buhler D, Wirth B, Sendtner M, et al. Co-regulation of survival of motor neuron (SMN) protein and its interactor SIP1 during development and in spinal muscular atrophy. Hum Mol Genet 2001;10:497–505.
Jahn R, Lang T, Sudhof TC. Membrane fusion. Cell 2003;112:519–33.
Kawaguchi Y, Hoshimaru M, Nawa H, Nakanishi S. Sequence analysis of cloned cDNA for rat substance P precursor: existence of a third substance P precursor. Biochem Biophys Res Commun 1986;139:1040–6.
Kong SK, Ko S, Lee CY, Lui PY. Practical considerations in acquiring biological signals from confocal microscope. Methods Enzymol 1999;307:20–6.
Kramer MS, Cutler N, Feighner J, Shrivastava R, Carman J, Sramek JJ, et al. Distinct mechanism for antidepressant activity by blockade of central substance P receptors. Science 1998;281:1640–5.
Kuriyan J, Eisenberg D. The origin of protein interactions and allostery in colocalization. Nature 2007;450:983–90.
Lakowicz J. Principles of Fluorescence Spectroscopy, 3rd ed. New York: Springer; 2006.
Landmann L, Marbet P. Colocalization analysis yields superior results after image restoration. Microsc Res Tech 2004;208:103–12.
LeDoux JE. Emotion circuits in the brain. Annu Rev Neurosci 2000;23:155–84.
Lichtman JW, Colman H. Synapse elimination and indelible memory. Neuron 2000;25:269–78.
Lisanti MP, Scherer PE, Tang Z, Sargiacomo M. Caveolae, caveolin and caveolin-rich membrane domains: a signalling hypothesis. Trends Cell Biol 1994;4:231–5.
Liu Q, Dreyfuss G. A novel nuclear structure containing the survival of motor neurons protein. EMBO J 1996;15:3555–65.
Manders EM, Stap J, Brakenhoff GJ, van Driel R, Aten JA. Dynamics of three-dimensional replication patterns during the S-phase, analysed by double labelling of DNA and confocal microscopy. J Cell Sci 1992;103:857–62.
Manders EMM, Verbeek FJ, Aten JA. Measurement of co-localization of objects in dual-colour confocal images. J Microscopy 1993;169:375–82.
Mantyh PW, Gates T, Mantyh CR, Maggio JE. Autoradiographic localization and characterization of tachykinin receptor binding sites in the rat brain and peripheral tissues. J Neurosci 1989;9:258–79.
McDonald JW, Johnston MV. Physiological and pathophysiological roles of excitatory amino acids during central nervous system development. Brain Res Brain Res Rev 1990;15:41–70.
Mokin M, Keifer J. Quantitative analysis of immunofluorescent punctate staining of synaptically localized proteins using confocal microscopy and stereology. J Neurosci Methods 2006;157:218–24.
Murry CE, Jennings RB, Reimer KA. Preconditioning with ischemia: a delay of lethal cell injury in ischemic myocardium. Circulation 1986;74:1124–36.

Nadrigny F, Rivals I, Hirrlinger PG, Koulakoff A, Personnaz L, Vernet M, et al. Detecting fluorescent protein expression and co-localisation on single secretory vesicles with linear spectral unmixing. Eur Biophys J 2006;35:533–47.
Nakamura K, Hioki H, Fujiyama F, Kaneko T. Postnatal changes of vesicular glutamate transporter (VGluT)1 and VGluT2 immunoreactivities and their colocalization in the mouse forebrain. J Comp Neurol 2005;492:263–88.
Nakamura K, Watakabe A, Hioki H, Fujiyama F, Tanaka Y, Yamamori T, et al. Transiently increased colocalization of vesicular glutamate transporters 1 and 2 at single axon terminals during postnatal development of mouse neocortex: a quantitative analysis with correlation coefficient. Eur J Neurosci 2007;26:3054–67.
Nakaya Y, Kaneko T, Shigemoto R, Nakanishi S, Mizuno N. Immunohistochemical localization of substance P receptor in the central nervous system of the adult rat. J Comp Neurol 1994;347: 249–74.
Nawa H, Hirose T, Takashima H, Inayama S, Nakanishi S. Nucleotide sequences of cloned cDNAs for two types of bovine brain substance P precursor. Nature 1983;306:32–6.
Ni B, Wu X, Yan GM, Wang J, Paul SM. Regional expression and cellular localization of the Na(+)-dependent inorganic phosphate cotransporter of rat brain. J Neurosci 1995;15:5789–99.
Nilsson G, Hokfelt T, Pernow B. Distribution of substance P-like immuno-reactivity in the rat central nervous system as revealed by immunohistochemistry. Med Biol 1974;52:424–7.
North AJ. Seeing is believing? A beginners' guide to practical pitfalls in image acquisition. J Cell Biol 2006;172:9–18.
Oberholzer M, Ostreicher M, Christen H, Bruhlmann M. Methods in quantitative image analysis. Histochem Cell Biol 1996;105:333–55.
Ostrom RS, Liu X, Head BP, Gregorian C, Seasholtz TM, Insel PA. Localization of adenylyl cyclase isoforms and G protein-coupled receptors in vascular smooth muscle cells: expression in caveolin-rich and noncaveolin domains. Mol Pharmacol 2002;62:983–92.
Oyler GA, Higgins GA, Hart RA, Battenberg E, Billingsley M, Bloom FE, et al. The identification of a novel synaptosomal-associated protein, SNAP-25, differentially expressed by neuronal subpopulations. J Cell Biol 1989;109:3039–52.
Oyler GA, Polli JW, Higgins GA, Wilson MC, Billingsley ML. Distribution and expression of SNAP-25 immunoreactivity in rat brain, rat PC-12 cells and human SMS-KCNR neuroblastoma cells. Brain Res Dev Brain Res 1992;65:133–46.
Oyler GA, Polli JW, Wilson MC, Billingsley ML. Developmental expression of the 25-kDa synaptosomal-associated protein (SNAP-25) in rat brain. Proc Natl Acad Sci U S A 1991;88:5247–51.
Pawson T, Scott JD. Signaling through scaffold, anchoring, and adaptor proteins. Science 1997;278: 2075–80.
Reiter HO, Waitzman DM, Stryker MP. Cortical activity blockade prevents ocular dominance plasticity in the kitten visual cortex. Exp Brain Res 1986;65:182–8.
Rubino A, Yellon DM. Ischaemic preconditioning of the vasculature: an overlooked phenomenon for protecting the heart? Trends Pharmacol Sci 2000;21:225–30.
Salter MW, Kalia LV. Src kinases: a hub for NMDA receptor regulation. Nat Rev Neurosci 2004;5: 317–28.
Sasagawa K, Matsudo Y, Kang M, Fujimura L, Iitsuka Y, Okada S, et al. Identification of Nd1, a novel murine kelch family protein, involved in stabilization of actin filaments. J Biol Chem 2002;277: 44140–6.
Schultz W. Behavioral dopamine signals. Trends Neurosci 2007;30:203–10.
Sedarat F, Lin E, Moore ED, Tibbits GF. Deconvolution of confocal images of dihydropyridine and ryanodine receptors in developing cardiomyocytes. J Appl Physiol 2004;97: 1098–103.
Sharma A, Lambrechts A, Hao le T, Le TT, Sewry CA, Ampe C, et al. A role for complexes of survival of motor neurons (SMN) protein with gemins and profilin in neurite-like cytoplasmic extensions of cultured nerve cells. Exp Cell Res 2005;309:185–97.
Shaw PJ, Rawlins DJ. The point spread function of a confocal microscope: its measurement and use in deconvolution. J Microsc 1991;163:151–65.
Shigematsu N, Yamamoto K, Higuchi S, Fukuda T. An immunohistochemical study on a unique colocalization relationship between substance P and GABA in the central nucleus of amygdala. Brain Res 2008;1198:55–67.
Smallcombe A. Multicolor imaging: the important question of co-localization. Biotechniques 2001; 30:1240–6.

Soriano FX, Papadia S, Hofmann F, Hardingham NR, Bading H, Hardingham GE. Preconditioning doses of NMDA promote neuroprotection by enhancing neuronal excitability. J Neurosci 2006; 26:4509–18.
Stryker MP, Harris WA. Binocular impulse blockade prevents the formation of ocular dominance columns in cat visual cortex. J Neurosci 1986;6:2117–33.
Sudhof TC. The synaptic vesicle cycle. Annu Rev Neurosci 2004;27:509–47.
Takamori S. VGLUTs: 'exciting' times for glutamatergic research? Neurosci Res 2006;55:343–51.
Tovar KR, Westbrook GL. The incorporation of NMDA receptors with a distinct subunit composition at nascent hippocampal synapses in vitro. J Neurosci 1999;19:4180–8.
Ungless MA, Whistler JL, Malenka RC, Bonci A. Single cocaine exposure in vivo induces long-term potentiation in dopamine neurons. Nature 2001;411:583–7.
Yong J, Wan L, Dreyfuss G. Why do cells need an assembly machine for RNA–protein complexes? Trends Cell Biol 2004;14:226–32.
Young PJ, Le TT, thi Man N, Burghes AH, Morris GE. The relationship between SMN, the spinal muscular atrophy protein, and nuclear coiled bodies in differentiated tissues and cultured cells. Exp Cell Res 2000;256:365–74.
Zhang H, Xing L, Rossoll W, Wichterle H, Singer RH, Bassell GJ. Multiprotein complexes of the survival of motor neuron protein SMN with Gemins traffic to neuronal processes and growth cones of motor neurons. J Neurosci 2006;26:8622–32.
Zinchuk O, Fukushima A, Hangstefer E. Dynamics of PAF-induced conjunctivitis reveals differential expression of PAF receptor by macrophages and eosinophils in the rat. Cell Tissue Res 2004;317: 265–77.
Zinchuk O, Fukushima A, Zinchuk V, Fukata K, Ueno H. Direct action of platelet activating factor (PAF) induces eosinophil accumulation and enhances expression of PAF receptors in conjunctivitis. Mol Vis 2005;11:114–23.
Zinchuk V, Zinchuk O. Quantitative colocalization analysis of confocal fluorescence microscopy images. Curr Protoc Cell Biol 2008 Unit 4.19.
Zinchuk V, Zinchuk O, Akimaru K, Moriya F, Okada T. Ethanol consumption alters expression and colocalization of bile salt export pump and multidrug resistance protein 2 in the rat. Histochem Cell Biol 2007a;127:503–12.
Zinchuk V, Zinchuk O, Okada T. Quantitative colocalization analysis of multicolor confocal immunofluorescence microscopy images: pushing pixels to explore biological phenomena. Acta Histochem Cytochem 2007b;40:101–11.